Assessing the activity and stability of Cu2O/SnO2-based gas diffusion electrodes for the CO2 conversion in different electrolytes: Bicarbonate vs. Ionic Liquid/Acetonitrile

Chemical Engineering Journal 514 (2025) 163265

Contents lists available at ScienceDirect

Chemical Engineering Journal

journal homepage: www.elsevier.com/locate/cej

Assessing the activity and stability of Cu_2O/SnO_2-based gas diffusion electrodes for the CO_2 conversion in different electrolytes: Bicarbonate vs. Ionic Liquid/Acetonitrile

Federica Zammillo [a,3], Hilmar Guzmán [a,3], Daniela Polino [b], Roger Miró [c], Alberto Lopera [d], Emmanuele Parisi [a], Alessia Fortunati [a,1], Maddalena Zoli [a,2], Elena Simone [a], Nunzio Russo [a], Mariajose López-Tendero [d], Miriam Díaz de los Bernardos [c], Giovanni M. Pavan [a,b], Simelys Hernández [a,e,*]

[a] Department of Applied Science and Technology (DISAT), Politecnico di Torino, C.so Duca degli Abruzzi, 24, 10129 Turin, Italy
[b] Department of Innovative Technologies, University of Applied Sciences and Arts of Southern Switzerland, Polo Universitario Lugano, Campus Est, Viala Santa 1, 6962 Lugano-Viganello, Switzerland
[c] Unitat de Tecnologies Químiques, Fundació Eurecat - Centre Tecnològic de Catalunya, Tarragona 43007, Spain
[d] Laurentia Technologies, Parque Tecnologico, Valencia 46980, Spain
[e] Clean Water Center (CWC) Politecnico di Torino, C.so Duca degli Abruzzi, 24, 10129 Turin, Italy

ARTICLE INFO

Keywords:
Gas diffusion electrode
Cu_2O/SnO_2 catalyst
IL-Acetonitrile electrolyte
Electrochemical CO_2 conversion
DFT
Flow cell
Catalyst stability

ABSTRACT

Gas diffusion electrodes (GDEs) are key components for enabling the deployment of electrochemical CO_2 conversion on a large scale. Most studies focused on optimising the GDEs' performance in aqueous electrolytes, while their use with non-conventional electrolytes integrating CO_2 capture and co-catalytic conversion abilities is missing in the literature. Herein, the performance of a newly designed Cu_2O/SnO_2-based GDE was investigated for the first time in a continuous-feed flow cell at a 10.2 cm^2 scale, both in an aqueous $KHCO_3$ medium and in a binary ionic liquid-organic solvent solution. Outstanding catalyst stability and selectivity, i.e. Faradaic efficiency to CO (FE_{CO}) from 84 to 90 % in the aqueous electrolyte, was demonstrated at current densities between −20 and −100 mA cm^{-2}, establishing a benchmark for the CO_2 reduction to CO on a Cu-based GDE. In comparison, a FE_{CO} of 35 % (CO/H_2 ratio > 3) was reached at –20 mA cm^{-2} with 1-Butyl-3-methylimidazolium triflate ([BMIM][TfO]) in acetonitrile (ACN). Still, stability issues and a performance drop were faced during operation in this aprotic media. Molecular dynamics simulations and ex-situ physical–chemical characterisation assessed that the changes in the catalyst/GDE structure and electrolyte properties started with the displacement of Cu surface atoms from their equilibrium position by ACN molecules, which promotes the subsequent dissolution of Cu in the presence of [BMIM][TfO] molecules. Our findings highlight the significant influence of electrolyte composition on catalyst surface transformation and performance during the reaction. This work unveils critical issues for the practical application of IL-based electrolytes as co-catalysts and CO_2 capture media for CO_2 electrochemical conversion systems and proposes some mitigation strategies.

1. Introduction

The rising concentration of CO_2 in the atmosphere, primarily due to

* Corresponding author.
E-mail addresses: federica.zammillo@polito.it (F. Zammillo), hilmar.guzman@polito.it (H. Guzmán), daniela.polino@supsi.ch (D. Polino), roger.miro@eurecat.org (R. Miró), alberto.lopera@laurentia.es (A. Lopera), emmanuele.parisi@polito.it (E. Parisi), alessia.fortunati@iit.it (A. Fortunati), maddalena.zoli@helmholtz-berlin.de (M. Zoli), elena.simone@polito.it (E. Simone), mlopezt@laurentia.es (M. López-Tendero), miriam.diaz@eurecat.org (M.D. de los Bernardos), giovanni.pavan@polito.it (G.M. Pavan), simelys.hernandez@polito.it (S. Hernández).
[1] Current Address: Istituto Italiano di Tecnologia, Via Livorno 60, 10144, Turin, Italy.
[2] Current Address: Helmholtz-Zentrum Berlin für Materialien und Energie, Hahn-Meitner-Platz 1, 14109, Berlin. Germany.
[3] These authors contributed equally to this work.

https://doi.org/10.1016/j.cej.2025.163265
Received 26 January 2025; Received in revised form 18 April 2025; Accepted 29 April 2025
Available online 30 April 2025

Nomenclature

Acronyms and abbreviations

ACN	Acetonitrile
AIMD	Ab initio molecular dynamics
BMIM	1-Butyl-3-methylimidazolium
CO_2R	Carbon dioxide reduction
CV	Cyclic voltammetry
CP	Chronopotentiometry
EC	Electrochemical
EDS	Energy dispersive X-ray spectroscopy
EIS	Electrochemical impedance spectroscopy
FCC	Face-centered cubic
FE	Faradaic Efficiency
FESEM	Field emission scanning electron microscopy
GDE	Gas diffusion electrode
GDL	Gas diffusion layer
HER	Hydrogen evolution reaction
IL	Ionic liquid
LSV	Linear sweep voltammetry
TEM	Transmission electron microscopy
TfO	Triflate
XRD	X-ray diffraction
WE	Working electrode

Parameters

E	Applied potential
ΔE	Energy difference
J	Current density
n_{ct}	Index of the constant phase element
R_{ct}	Charge transfer resistance
Q_{ct}	Capacitance of the constant phase element
τ_{ct}	Charge transfer time constant

hydrocarbon combustion, has increased from 280 ppm to over 400 ppm since the Industrial Revolution, posing a threat to global security.[1,2] Transitioning to a carbon–neutral economy is urgent. Using CO_2 as a feedstock can support this transition, with electrochemical (EC) CO_2 conversion emerging as a promising method due to its lower energy requirements and in-loco hydrogen production from water.[3,4] However, challenges remain, such as achieving low overpotentials, high current densities, selectivity, and stable long-term operations.[5].

Alongside the essential role of the electrocatalyst, it is widely recognised that identifying an optimal electrolytic solution could promote selectivity toward a target product.[6,7] In this regard, inorganic aqueous solutions have been traditionally used as electrolytes due to their relatively low cost and wide availability.[8–12] However, the low CO_2 solubility in water-based solutions limits the reaction rates to lab scale-relevant values.[13–15] The competing hydrogen evolution reaction (HER) can also negatively affect the reaction selectivity towards carbon products in aqueous conditions. The solubility of CO_2 can be markedly increased in organic solvents: combined with the absence of protons from water, this can translate into higher production rates towards the CO_2 reduction (CO_2R) products. Nonetheless, their high cost, volatility, flammability and toxicity are not negligible aspects.[6,16,17].

Recently, ionic liquids (ILs) have attracted great interest as electrolytes for CO_2R due to their high CO_2 absorption capacity, negligible vapour pressure and promising co-catalytic properties.[18–20] Generally, they consist of an organic cation and an inorganic anion. These unique salts are emerging as a viable alternative to organic solvents for electrocatalysis. The catalytic-promoting effect of this class of compounds was reported in a recent work by Rosen *et al.*, where the synergistic effect between a stable silver electrode and an aqueous solution of 1-Ethyl-3-methylimidazolium-tetrafluoroborate ([EMIM][BF_4]) for the reduction of CO_2 to carbon monoxide (CO) was demonstrated, achieving a Faradic Efficiency (FE) of over 96 % at a cathodic current density lower than 7 mA cm^{-2} and low overpotential.[21] However, important drawbacks limit the ILs' practical application: high cost and viscosity. In particular, the high viscosity, which depends on the length of the alkyl chain and the anion's nature, complicates the IL usage in the existing equipment. Adding cosolvents, like water or organic solvents, is suggested to overcome the viscosity issue.[22,23] Interestingly, the binary aqueous/organic solvent-IL solutions may also represent an efficient medium for CO_2 electroreduction, as proven among others by Rosen and co-workers.[19,21,24–26] The benefit of ILs' enhanced CO_2 solubility in gas-fed continuous flow cells may seem diminished given the excess CO_2 supply. However, the rationale for studying ILs in this context goes beyond solubility. ILs offer distinct advantages, including modifying the electrochemical environment by activating CO_2, stabilising key intermediates, and adjusting local pH, which can enhance product selectivity.[27] Despite challenges like cost and viscosity, ILs remain promising candidates for optimising CO_2 conversion systems, given their broader functional benefits.[28–30] Achieving high current density with ILs is, however, uncommon. A new ionic liquid N-octyl-trimethyl ammonium 1,2,4-triazole ([N1118][TRIZ]) was designed and allowed Hu and colleagues to reach a current density up to 50.8 mA cm^{-2} with a FE_{CO} of about 90 % in an H-type cell, using a commercial Ag plate as the working electrode.[31] Instead, a flow-through electrode geometry was conceived to overcome the mass-transport limitations associated with the dissolution of CO_2 in the bulk of IL electrolytes. A system based on an Ag-coated macroporous aluminium foam with a geometric surface area lower than 0.5 cm^2 was examined. Flowing the aqueous [EMIM][BF_4] mixture along the electrode/electrolyte interface aided in reducing the diffusion layer thickness and increased the maximum current density up to 50 mA cm^{-2} with FE_{CO} of 75 % compared to about 6 mA cm^{-2} reached in static conditions.[32] Rosen et al. were the first to run ILs-based experiments in a flow cell, employing a silver-based-gas diffusion electrode (GDE) with an active area of 1.5 cm^2. GDEs in CO_2RR allow high selectivity and commercially relevant current densities in aqueous electrolytes.[14] Nevertheless, current densities with organic-based solvents are limited to around 50 mA cm^{-2}, both because higher overpotentials are required (which also contribute to the systems' instability) and because few investigations employing GDEs in aprotic solvents are reported in the literature. Additionally, stability studies are in their infancy, and the scale-up of the electrodes needs to be tested.[33].

Copper-based electrocatalysts are extensively studied because of their promising properties for EC CO_2R. However, the relative unselectivity of these materials represents one major drawback. In this sense, in 2017, Huan *et al.* demonstrated the importance of the media in orienting reaction selectivity. Specifically, a porous and dendritic electrodeposited Cu on a Cu plate displayed high selectivity for formate in [EMIM][BF_4], in the presence of water. A stable performance in a two-chamber cell with a Faradaic yield for formate of 87 % over an 8-hour long-term test with a 1 cm^2 electrode.[34] Sputtered CuSn thin film alloys on Ni foils were investigated in acetonitrile (ACN)/imidazolium-based electrolytes by Rosenthal and collaborators.[35] In a two-compartment cell, the CuSn cathode materials reported a maximum FE_{CO} of 41 %, with a minimal H_2 production. Nonetheless, the state-of-the-art shows a knowledge gap in exploring copper-based GDE's performance in the presence of ILs as electrolytes or electrolyte additives.[36] On the other hand, many works have investigated the effect of ILs as direct modifiers of the Cu-electrode surface. For example, Sha and co-workers modified the reaction microenvironment of a Cu-based catalyst

by anchoring 1-butyl-3-methylimidazolium nitrate, [BMIM][NO_3]. This led to the optimisation of Cu atomic coordination and electronic properties, enabling a high FE of 77.3 % toward ethylene in $KHCO_3$ aqueous solution using an H-type cell.[37] Likewise, more recently Cai *et al.* introduced 1-butyl-3-methylimidazolium hexafluoro-phosphate, [BMIM][PF_6], by drop-casting the IL onto synthesised Cu nanowires. Their work highlighted the IL's ability to trap key intermediates, break the coupling process toward ethylene production, and steer the reaction pathway to methane. Thus, the main products could be switched between C_2H_4 with a 71 % FE and CH_4 with a 67 % FE by simply modifying the copper catalyst interface.[38] Also noteworthy is the study conducted by Garcia and collaborators on the solvent effect on the CO_2R performance of a nanostructured Cu electrode. The EC CO_2R in ACN was shown to be structure-dependent. Nanocube-covered copper was the only surface capable of producing ethylene with a 10 % FE, in the presence of a certain amount of water. CO was the main product in the organic medium, with FE > 85 %, but the measurements were carried out in a single-compartment EC cell, with a polycrystalline Cu disk or Cu_xO used as the cathode.[39].

The use of aprotic media in the electroreduction of CO_2 opens up alternative avenues for this technology, like producing oxalic acid, ethylene glycol or methyl formate.[7,40] Moreover, the studies in non-aqueous environments offer the potential to functionalise the CO_2-derived product via integrated and single-pot approaches, like coupling to carbonylation chemistry or hydroformylation processes (i.e., SunCo-Chem project).[28,41–43] In this regard, the selective conversion of CO_2 to CO would, for example, ensure an important building block for synthesising bulk and fine chemicals. Nonetheless, deploying these reactions on a large scale requires developing continuous flow reactors to maximise the energy efficiency of the whole process. Another advantage of using ILs-based electrolytes is their capture capacity, which can be fine-tuned to boost the single-pass conversion of CO_2 and recirculate the unconverted CO_2.

Many studies have reached Faradaic efficiency (FE) toward CO over 80 % in aqueous electrolytes to date, in some cases demonstrating the performance at industrial relevant industrial-relevant current densities ($\geq$ 100 mA cm^{-2}) and low cell potentials ($\leq$ 3 V).[44,45] Almost all of these efforts have been conducted on Ag, well known for its CO-selectivity. However, there is a need to develop earth-abundant and noble-free metals to obtain cost-effective catalysts and make the process economically more attractive. Early demonstrations of highly CO-selective bimetallic Cu/Sn catalysts have been reported mainly at low current density in aqueous H-cell reactors.[46] Nonetheless, a later work investigated the performance of a Sn/Cu-based GDE in a zero-gap configuration and reported FE_{CO} above 80 % at 125 mA cm^{-2}, but using an electrode with an exposed area of only 0.196 cm^2.[47] Some of us have previously shown a highly selective conversion of CO_2 to CO on Ag foil in the presence of a [BMIM][TfO] solution in ACN.[48] Herein, for the first time, the performance of the [BMIM][TfO] in ACN electrolyte was investigated within a continuous-fed electrochemical cell over copper/tin oxide-based GDEs with an active area of 10 cm^2. Our research aims to systematically address the challenges of employing ILs and investigate whether those can be engineered for practical application in continuous-flow, gas-fed systems. Different reactor configurations were explored here to increase CO_2 availability at the catalyst surface. Among these, a two-compartment layout was the most promising. This work exposes the limitations of carbon-based gas diffusion layers (GDLs) in organic solvents. Indeed, the Cu_2O/SnO_2-based catalyst supported on carbon paper showed outstanding stability in aqueous media but faced stability issues and performance drops in the aprotic environment. The blackening of carbon paper and colour changes of the electrolytes were evidenced as degradation phenomena, undermining the selectivity of the process and limiting the prospects of scalability. To figure out ways to solve such issues, we conducted a deeper investigation. We demonstrated from both experimental and theoretical points of view that the deterioration of the system originates from the strong affinity between the IL/ACN electrolyte and Cu at the −catalyst surface, which means that the electrolyte solvent must be appropriately tuned or other strategies, such as introducing an ionomer coating or alloying with second metals, should be envisaged to ensure long-term stability in the aprotic media.

2. Materials and methods

2.1. Materials

Copper nanopowder (40–60 nm particle size (SAXS), ≥99.5 % trace metals basis, Sigma Aldrich). ZnO (20–25 nm particle size from Sigma Aldrich). Nafion perfluorinated resin solution Green Alternative (5 wt% in lower aliphatic alcohols and water contains 15–20 % water from Sigma Aldrich). Potassium bicarbonate (99.7 % from Sigma Aldrich). Potassium hydroxide (≥85 %, pellets from Sigma Aldrich). Ethanol (≥99.8 % from Sigma Aldrich). Acetonitrile anhydrous (99.8 % from Sigma Aldrich). Sulfuric acid (95–97 % from Sigma Aldrich). Toray carbon paper (TGP-H-060), Sigracet 39BC and bipolar membrane Fumasep were purchased from the FuelCell Store. 1-butyl-3-methylimidazolium trifluoromethanesulfonate ([BMIM][TfO], 99 %) was supplied by IOLITEC GmbH. All chemical materials were used without further purification. All the aqueous electrolyte solutions were prepared using ultrapure water (18.2 MΩ cm^{-1} resistivity).

2.2. Preparation of the gas diffusion electrodes

The copper-based GDEs with a catalyst loading of 1 mg cm^{-2} were prepared by depositing a catalytic ink on a porous carbon paper using an airbrushing technique. The catalytic ink comprised different components: (i) Cu_2O/SnO_2-based nanoparticles, consisting of Cu_2O/SnO_2 powder functionalised with VTES, and Ru and Re complexes deposited through electropolymerisation, unless otherwise stated – the detailed preparation of which is provided in the Supporting Information (SI) (see section S1, Table S1, Scheme S1–S3, Figs. S1–S4);[27] (ii) Nafion (dispersion, 5 %wt in water and 1-propanol) as the binder for the catalyst particles and to ensure ions transport within the electrode; (iii) ethyl alcohol, as the liquid carrier for the ink deposition. Where noted, CuZn-based nanoparticles were employed as catalysts.[49] Each Cu-based GDE was prepared with a geometric area of 10.2 cm^2. The carbon paper sheets were coated on a heating plate to ensure complete solvent evaporation. It is important to note that the multi-step synthesis and the airbrushing deposition technique introduced complex conditions—such as redox reactions in the organic electrolyte and exposure to varying potentials—that can contribute to the formation of mixed copper species. These conditions impact the final composition of the catalyst layer and play a significant role in the structural and electrochemical behaviour of the Cu-based GDEs.

2.3. Electrochemical cell and experimental conditions

An ElectroCell Micro Flow Cell® was used to assess the performances of the prepared GDEs. An Ir-MMO plate was employed as the anode, and a leak-free Ag/AgCl was used as the reference electrode (RE). Unless otherwise stated, the RE was inserted in the anodic compartment. This arrangement was chosen to minimise contamination risks and maintain the integrity of the electrolyte in the cathodic compartment. Ag/AgCl reference electrodes can be used in some ionic liquids; however, the high solubility of AgCl in some ionic liquids dramatically limits their use. Non-aqueous Ag/$AgNO_3$ could alternatively be used, as it is compatible with organic media; however, design constraints of the cell limited its adoption in the flow cell. The cathodic GDE was used as the working electrode (WE) with an active area of 10 cm^2. A three-compartment or two-compartment configuration (Fig. 1) was employed to run the electrochemical measurements. In the former case, the WE was exposed, on one side, to the catholyte and, on the other side, to the CO_2 gaseous

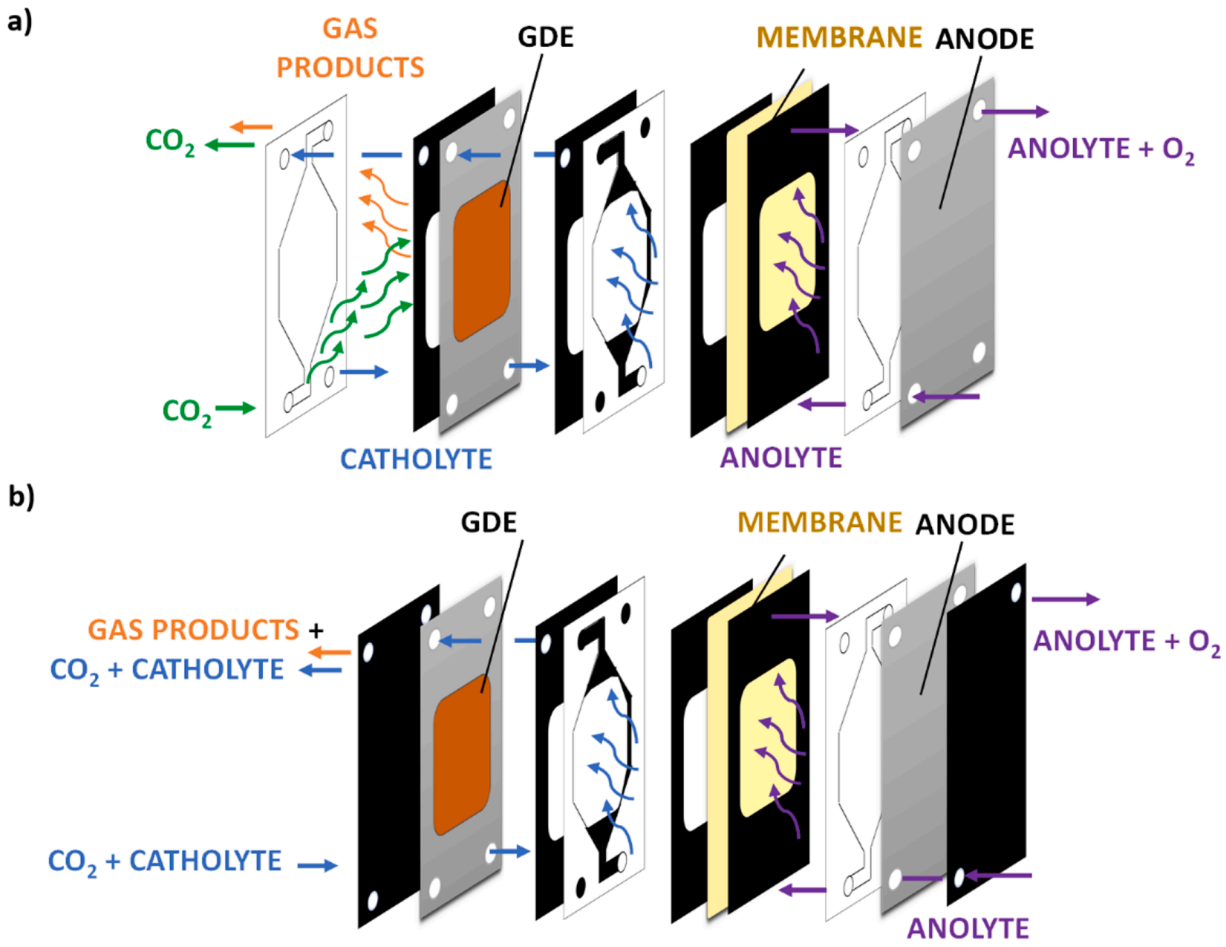

Fig. 1. Schematic layouts of the three-compartment (a) and two-compartment (b) cell configurations.

stream. Instead, the two-compartment cell was operated, placing the GDE on a conductive titanium plate, acting as the current collector, and exposing the active area of the GDE to a CO_2-saturated catholyte.

The catholyte, 0.1 M $KHCO_3$ aqueous solution or 0.3 M [BMIM][TfO] in ACN, was circulated at 26.5 mL min^{-1}. An aqueous solution of 0.1 M KOH was employed as the anolyte, circulated at 45 mL min^{-1} employing a peristaltic pump. Both streams needed two external 30 mL reservoirs. The CO_2 flow rate was set at 20 and 10 NmL min^{-1} for the three-compartment and two-compartment configurations, respectively. When required, a bipolar membrane was used in reverse-bias mode to separate the cathodic and anodic chambers, thereby enabling pH control in both compartments and to enhance the syngas productivity in $KHCO_3$-based aqueous electrolyte in comparison to an anion exchange membrane (see section S4 in the SI). The electrochemical cell was operated at ambient conditions, controlling an overpressure of 10 mbar at the outlet gas products stream. The inline gas products analysis was carried out by using a micro gas chromatograph (Agilent 990 Micro GC, equipped with Molsieve 5Å and Pora PLOT U capillary columns). Formate quantification was performed using a high-performance liquid chromatography (Shimadzu HPLC, Prominence model with detector RID-10A, SPD-M20A, ELSD-LT II and RF-20A). Samples of the liquid products were analyzed at the beginning and at the end of each experiment. Volatile organic products were analysed using a gas chromatograph (Perkin Elmer GC with a mass spectrometer) with a headspace.

The Faradaic efficiency, i.e. efficiency of the electron transfer, was determined by using the following Eq. (1):

$$FE(\%) = \frac{z \bullet \dot{n} \bullet F}{j \bullet A \bullet t} \times 100 \quad (1)$$

where z represents the number of electrons exchanged by each half-reaction at the cathode surface, $\dot{n}$ is the outlet molar flow rate of the product (e.g. CO, H_2, formate), j is the current density, t is the reaction time, F is the Faraday constant, and A is the active geometric area (10.2 cm^2).

A multichannel potentiostat (BioLogic VSP-300) was used for the electrochemical measurements. Each GDE was first subjected to Cyclic Voltammetry (CV) in N_2 and CO_2 environments to assess its stability and compare the activity under inert and reactive atmospheres. Then, the electrochemical activity of the GDE was evaluated with a Linear Sweep Voltammetry (LSV) by scanning the potential up to reach this study's target current density value: –20 mA cm^{-2}. Finally, galvanostatic measurements (chronopotentiometry, CP) at –20, –50 or –100 mA cm^{-2} were carried out to evaluate the selectivity and stability of the investigated systems.

2.4. Characterisation techniques

2.4.1. Field emission scanning electron microscopy (FESEM) with EDX

Field Emission Scanning Electron microscopy (FESEM) analytical technique, operated at 3 kV, was employed to obtain information about the morphology of the samples. To this purpose, two different instruments were used: a ZEISS Supra 40 and ZEISS MERLIN. Both instruments are equipped with an Energy Dispersive X-ray Spectroscopy System (EDS), which helps study the content of the relative elements of the samples. The samples were prepared by placing them on electrically conductive, non-porous carbon tapes before the FESEM analysis.

2.4.2. X-ray diffraction analysis

X-Ray Diffraction (XRD) technique was used to obtain information about the crystallinity of the samples by using a diffractometer (Panalytical X'Pert PRO) using monochromatic Cu-Kα radiation at 40 kV and 40 mA. XRD experiments utilised a PIXcel1D X-ray detector. The electrodes were scanned in grazing incident configuration with the X-ray source at a fixed 0.5° omega in the 2θ range of 25-80° with a scanning step of 0.020° and acquisition time of 8 s per step.

2.4.3. Raman spectroscopy

All Raman spectra were recorded at Room Temperature (298 K) using a Horiba LabRAM HR Evolution Raman microscope with a 100 mW diode laser source operating at 785 nm and 1064 nm. Solutions of [BMIM][TfO] in ACN were analysed in quartz cuvettes with a multichannel CCD Camera Symphony II Linear InGaAs Array detector, 300R/mm resolution grating. Backscattered radiation of carbon fibres was collected with a Synapse Plus BIDD Detector (1024 x 256 pixels), using a 300R/mm resolution grating. All the spectra were collected using 5 s exposure time, and 20 spectra were averaged for each sample analysed. To establish the homogeneity of solid samples, five measurements were collected at different points of the analysed surface. Spectra were smoothed and baseline corrected using the LabSpec 6 software; additionally, each spectrum was normalised with respect to the intensity of the G band peak (which was the highest in intensity for all samples analysed). Pre-processed spectra were analysed in Origin 2021, where Gaussian functions were used to fit the carbon peaks and extrapolate quantitative data (e.g., height).

2.4.4. Theoretical simulations

It was performed ab initio molecular dynamics (AIMD) simulations of a Cu (111) and a Cu_2O (100) surface in contact with a solution of [BMIM][TfO] in ACN at different concentrations to find out whether the interactions between the solution and the catalyst can modify the surface, inducing a performance loss. AIMD simulations were carried out using Quickstep, part of the CP2K package.[50] The Born–Oppenheimer forces were used to propagate the nuclear dynamics in these calculations. A 1×10^{-7} a.u. convergence criterion was used to optimise the wave function. The PBE exchange–correlation density function was employed to evolve the dynamics of the systems.[51] The m-DZVP Gaussian basis set and a plane wave cutoff of 450 Ry for the density were used.[52] Core electrons were treated using the Goedecker–Teter–Hutter (GTH) pseudopotentials.[53,54] The time step used was 1 fs. Production runs were carried out for 5 ps at 300 K in the NVT ensemble using the stochastic velocity-rescaling thermostat of Bussi et al.[55].

2.5. Electrochemical impedance spectroscopy

A one-compartment electrochemical cell was used to study the GDE/electrolyte interface through impedance spectroscopy. It comprised a three-electrode system, where the GDE (1 cm^2 area exposed) and a platinum coil were used as working and counter electrodes, respectively. A non-aqueous $Ag/AgNO_3$ reference was used for the measurements in the organic environment, whereas Ag/AgCl was employed in the aqueous solution. The EIS measurements were conducted in the 0.1 Hz to 0.2 MHz frequency range, with an amplitude of 10 mV and under different applied potentials in the −1 V to −2 V vs. Ag/Ag^+ range. EIS spectra were collected after specific electrochemical steps, namely after LSV, CP at –10 mA cm^{-2} and CP at 20 –mA cm^{-2}, in order to study the evolution of the electrochemical interfaces over time and after subjecting the system to different reaction conditions in both CO_2-saturated protic (0.1 M $KHCO_3$ aqueous solution) and aprotic (0.3 M [BMIM][TfO] in ACN) environments.

3. Results and Discussions

3.1. Electrochemical measurements

3.1.1. From batch to continuous reactors

A transition from batch to continuous reactors was initiated in this study to promote EC CO_2R at high rates and low overpotentials. In H-cell, the conversion of CO_2 on Ag foil (a CO-selective material) and in the presence of a non-aqueous electrolyte effectively improved the efficiency of CO_2 reduction products. Indeed, upon increasing the current density in both 0.1 M $KHCO_3$ aqueous electrolyte and 0.3 M [BMIM][TfO] in ACN electrolyte, a FE toward CO of about 80 % was preserved in the latter case (**Fig. S5** in the SI). On the contrary, with a water-based solution, the CO_2R selectivity decreased in favour of H_2 evolution at high overpotentials. This finding can be related to a limitation in CO_2 transport at high rates, as the C-source is at a much lower concentration than the proton donor (water).[56] It also demonstrates one of the main advantages of operating with organic-based systems: these solvents have lower proton concentrations, which allows them to suppress the competitive HER.

A comparative study was undertaken in GDE-cell – where transport limitations are overcome by directly feeding gaseous CO_2 to the electrode surface – to assess the activity of the synthesised Cu_2O/SnO_2-based catalyst in the presence of protic and aprotic solvents. Therefore, in a three-compartment configuration, the Cu_2O/SnO_2-based GDE was tested in a 0.1 M $KHCO_3$ aqueous electrolyte and in 0.3 M [BMIM][TfO] in ACN. The comparison between the linear polarisation curves in both electrolytes is shown in Fig. 2, showing the advantage of the IL-ACN environment in reducing the cathodic overpotential. However, constant-current electrolysis showed that the selectivity of the Cu_2O/SnO_2-GDE was significantly better in $KHCO_3$ at –20 mA cm^{-2}. As depicted in Fig. 3**a**, the $FE_{CO} > 70$ % obtained in the aqueous electrolyte was ten-fold higher than that of H_2, requiring a potential of approx. –4.5 V vs. Ag/AgCl (see Fig. 3**b**). Although the measured potential might appear unexpectedly high, it must be noted that this value includes the overpotential due to the bipolar membrane[57] – known to suffer from high ohmic resistance compared to the monopolar counterpart – and partially to the anolyte solution. Indeed, as specified in Section 2, the reference electrode was placed in the anodic chamber for these tests. With regard to the membrane aspect, a control experiment using an anion exchange membrane was conducted to address the cell potential issue; however, the productivity toward syngas was significantly

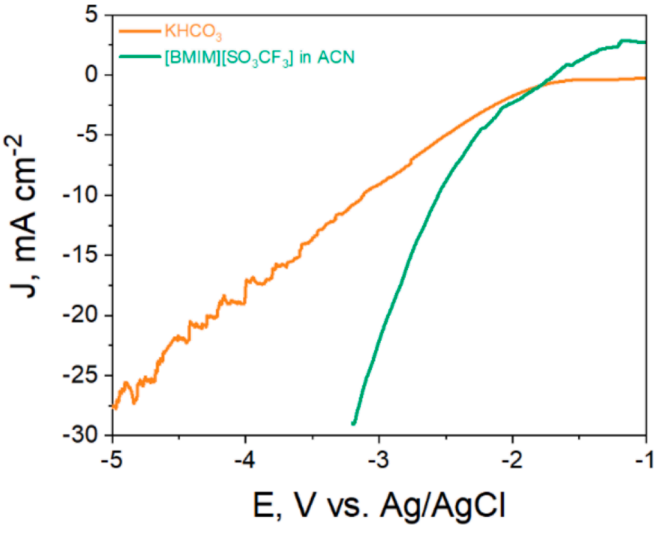

Fig. 2. Linear Sweep Voltammetry curves of a Cu_2O/SnO_2-GDE tested in both 0.1 M $KHCO_3$ and 0.3 M [BMIM][TfO] in ACN solution in three-compartment configuration. Reference electrode in the anolyte chamber.

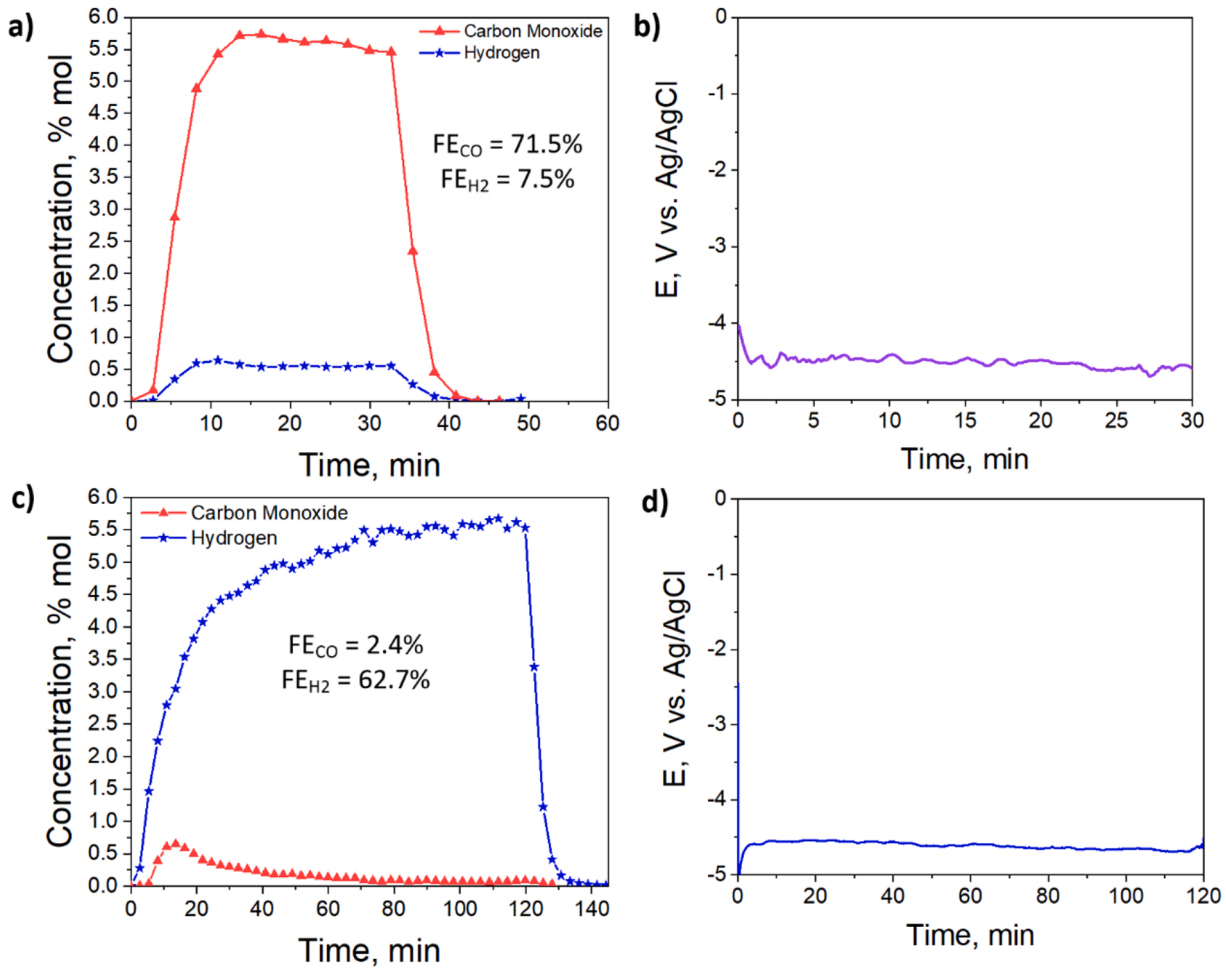

Fig. 3. Products trend (a, c) during chronopotentiometry measurement (b, d) performed at −20 mA cm^{-2} on Cu_2O/SnO_2-GDE in $KHCO_3$ 0.1 M (a,b) and 0.3 M [BMIM][TfO] in ACN (c,d) electrolytes, in a three-compartment configuration. Reference in the anolyte chamber.

compromised (see Fig. S6, SI).

On the other hand, an almost immediate fall in CO production was observed in the organic environment, with a final FE_{CO} > 2 % and a constant H_2 formation with a FE of around 63 % (Fig. 3**c**). Nonetheless, the CP measurement highlighted an inconsistency in the potential necessary for the reduction process at –20 mA cm^{-2}. Indeed, contrary to what could be expected from the current–potential dependence (Fig. 2), a higher potential was required to sustain the galvanostatic measurement (Fig. 3**d**). It might suggest a resistance increase either in the transport of CO_2 at the active sites or in the electrolyte over time. In this regard, the IL-ACN penetration within the porosity of the GDE, triggered by electrolysis, probably introduced a limitation to CO_2 diffusion from the gas bulk.[58] In fact, the electrolyte crossover from the catholyte chamber to the gas chamber could be experimentally corroborated by a partial collapse of the catalytic layer in the GDL structure (see section 3.2.1). Furthermore, studies revealed that the presence of water traces – which in this case could come from the wet membrane – can lead to the decomposition of acetonitrile into acetamide and to the formation of (bi) carbonates from CO_2, which can also justify the increase in the resistance of the electrolyte solution.[56,58,59].

3.1.2. Benchmarking the Cu_2O/SnO_2 catalyst performance in aqueous medium

Given the encouraging performances highlighted in the aqueous electrolyte, both in terms of FE and impedance response, the Cu_2O/SnO_2-based GDE was optimised to withstand longer operations. Indeed, the Toray carbon paper was replaced by a more hydrophobic substrate (Sigracet 39BC) to enhance the GDE's resistance to the aqueous electrolyte perspiration.[60] Coherently, with the higher hydrophobicity, an improvement in the CO_2 transport throughout the electrode's porosity can be expected, and thus, a higher CO_2R activity.

As shown in Fig. 4, the optimised Cu_2O/SnO_2-based GDE demonstrated remarkable stability, sustaining a very high selectivity toward CO (FE ~90 %) at –20 mA cm^{-2} for 24 h, with a calculated cathodic potential of –2 V vs. Ag/AgCl. The gaps observed in Fig. 4, precisely, between 250 and 500 min and around 750 min, result from deliberate pauses in the system's operation. These interruptions were implemented to manage and mitigate the potential effects of contaminant accumulation on the electrode surface. During these intervals, the system was temporarily switched off, and recovery procedures were carried out to restore electrode performance and selectivity. Over extended operation, contaminants from the electrolyte solution can compromise electrode activity and selectivity. To address this challenge, we developed electrode recovery protocols, combining electrochemical activation with rinsing procedures to remove accumulated impurities and help maintain optimal electrode functionality. These methods restore electrode performance without compromising long-term stability. A few studies producing CO/syngas indeed proved device durability greater than 1000 h,[61] but this lies outside the scope of the present work. Most importantly, it is noteworthy that such a high FE toward CO was obtained over a Cu-based GDE, while, typically, only noble metals like Au and Ag can produce CO at high faradaic efficiencies.[62].

The choice of − 20 mA cm^{-2} was aligned with the objectives of the SunCoChem project, as well as the catalyst material (see Fig. S7),[42]

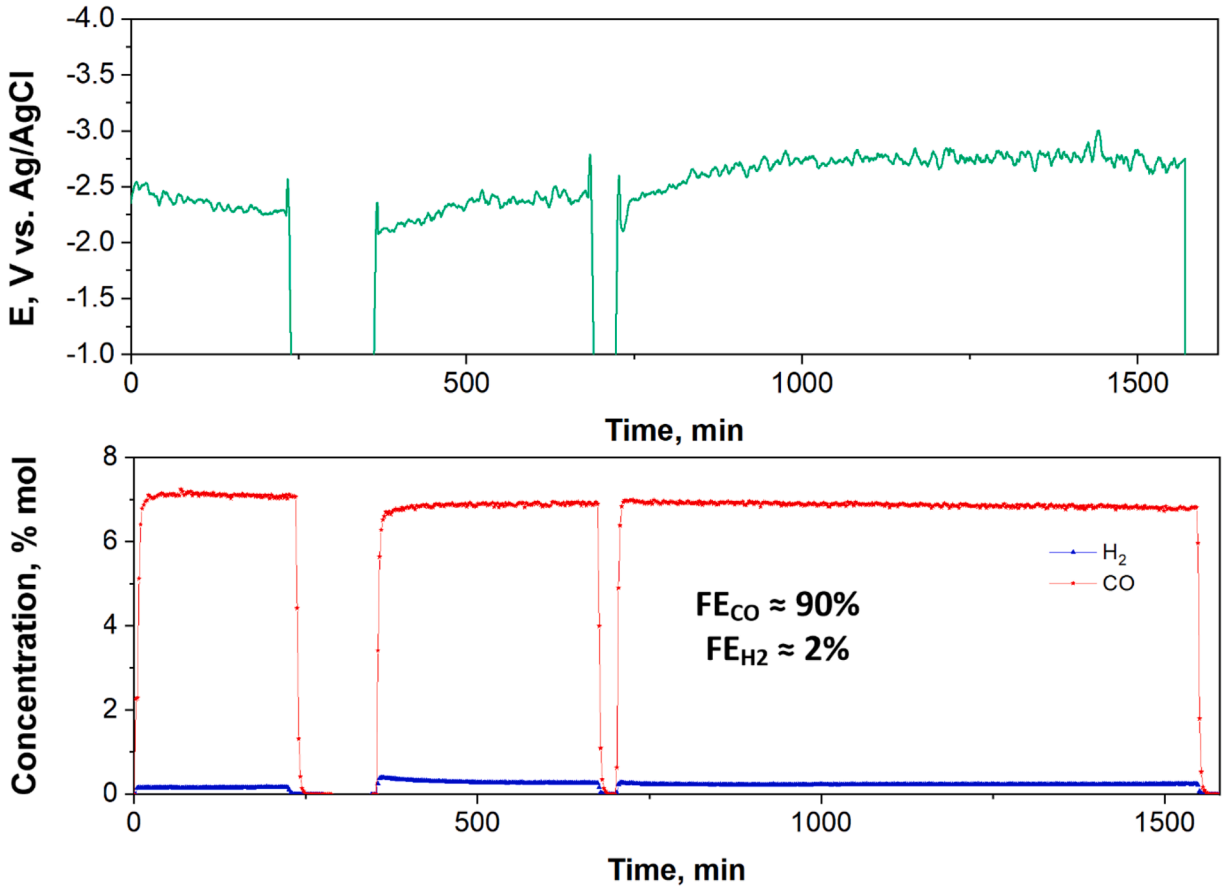

Fig. 4. Chronopotentiometry a) and products trend b) at −20 mA cm^{-2} on Cu_2O/SnO_2- GDE in $KHCO_3$ 0.1 M electrolyte during 24 h of operations. Reference electrode placed in the catholyte chamber.

which developed a TRL5 prototype that integrates CO_2 capture with photoelectrochemical conversion for on-site syngas production. The system was specifically designed to support downstream applications, such as the hydroformylation reaction employed by a company to manufacture fragrance components like Limoxal. Since the prototype operates with sunlight as the primary energy source, the target current density was intentionally moderated to reflect realistic operating conditions for solar-powered processes. Nonetheless, we recognise the importance of exploring higher current densities to broaden the applicability and relevance of our findings in diverse electrochemical settings. In response, we conducted additional investigations at higher current densities. These additional experiments, included in the SI (see **Fig. S8**), provide a more comprehensive understanding of the system's performance under more intense operational conditions, offering insights into the catalyst's robustness and selectivity beyond the original design constraints. We achieved 89 % and 84 % of FE for CO production at industrially relevant current densities (of 50 and 100 mA cm^{-2}, respectively) with an abundant and affordable catalyst. A small amount of formate was also produced, with an FE of about 1 % and 5 %, respectively. To mitigate high registered working potentials during these additional experiments, we kept the reference electrode in the 0.1 M $KHCO_3$ solution within the cathodic compartment. This adjustment aimed to lower the observed working potentials (approximately –3.5 and –4.5 V vs. Ag/AgCl at –50 and –100 mA cm^{-2}, respectively), enhancing the reliability of our measurements at elevated current densities.

3.1.3. *Facing stability issues in organic medium*

Despite the operation with GDEs, the initial findings highlighted CO_2 transport limitations in the presence of the IL-based electrolyte. Accordingly, a new continuous flow configuration was devised based on the H-cell concept. The CO_2 flux was bubbled into the catholyte flask, and the saturated catholyte was continuously fed in the cathodic chamber (see Fig. 1**b**). LSV curves in N_2-saturated and CO_2-saturated electrolytes (see **Fig. S9** in the SI) demonstrate that CO_2R activity prevails over HER. The two-compartment configuration facilitated the CO_2 reduction reactions on the Cu_2O/SnO_2-GDE at –20 mA cm^{-2} since an initial CO to H_2 ratio higher than 3 was obtained, with an estimated FE_{CO} of about 35 % in the first 40 min of testing (see Fig. 5**a**). However, the product trend shows that the system's stability was compromised after a while. Therefore, H_2 became the major product, as could be inferred from the simultaneous and slight decrease in the required potential after the first hour (see Fig. 5**b**). Moreover, a darkening of the electrode on both sides (see **Fig. S10** in the SI) and a colour change in the electrolyte could be observed after the test. That behaviour could be ascribed to the catalyst deactivation and degradation of the carbon paper due to the interactions between the IL-organic solvent electrolyte and the GDE.

A recent study on bimetallic catalysts discovered a structural evolution of an AgCu material, consisting of an Ag-core surrounded by a Cu_2O-shell.[63] The instability of the nanoparticles was investigated via transmission electron microscopy (TEM) under CO_2R conditions. The porous structure of the copper-based shell underwent morphological changes, and a loss of the core–shell structure was even evidenced at the highest overpotential values (from −500 mV to −800 mV vs. RHE). However, employing *ex situ* TEM measurements, they could understand that their observations resulted from a combined effect of high overpotentials and high local concentrations of CO originating at the Ag-sites. The easier access of CO_2 to Ag enhanced the CO formation, which eventually triggered an asymmetric reconstruction of the particles and caused the collapse of the entire core–shell structure. Therefore,

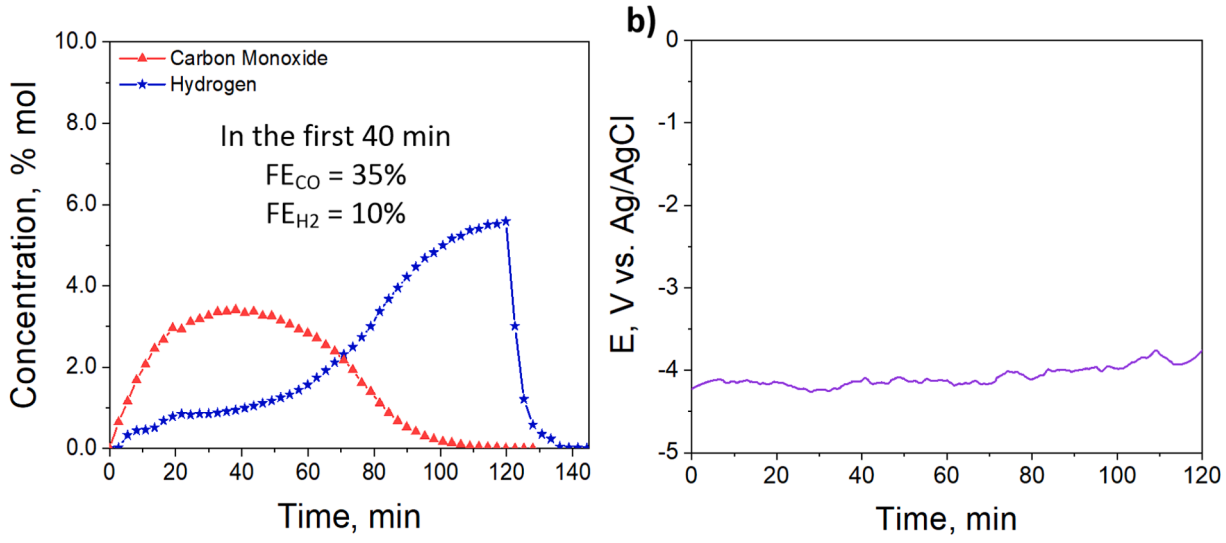

Fig. 5. Gaseous products trends (a) during chronopotentiometry measurement (b) performed at −20 mA cm^{-2} on Cu_2O/SnO_2-GDE in 0.3 M [BMIM][TfO] in acetonitrile electrolyte, in a two-compartment configuration. Reference in the anolyte chamber.

it could be assumed that the rough SnO_2 shell of the Cu_2O/SnO_2 nanoparticles, in which the Ru and Re complexes are deposited, initially providing the CO selectivity to the catalyst, suffers from interactions with IL-organic solvent, whose metal extraction capacity was discussed in the literature.[64,65] This may expose the copper oxide core to the electrolyte and eventually cause the deactivation of the catalytic system. Moreover, structural transformations of Cu NPs may occur under CO_2RR conditions, adversely affecting the activity.[66] At low overpotentials, particle migration and coalescence (PMC) govern the restructuring of the nanoparticles. The Ostwald ripening process becomes the dominant degradation mechanism at higher applied potentials. Strategies, such as introducing an ionomer coating or alloying with second metals, should be considered to meet the stability requirements. The work carried out by Kim et al. demonstrates that the rational design and implementation of a composite ionomer layer can tune the activity and selectivity of a Cu electrode, by controlling the local pH and CO_2 availability.[67] With specific regards to our Cu/Sn-based system, knowing that the catalyst surface is restructured under electrochemical operating conditions, a rational-designed ionomer coating can prevent those local conditions that facilitate the degradation mechanisms. Additionally, it may act as a barrier to IL-induced metal extraction. The extent of the degradation depends on the ranges of applied potentials. Alloying has been proposed as a further strategy to improve the Cu stability toward dissolution during CO_2 electroreduction. Okatenko *et al.* demonstrated that alloying Cu nanoparticles with Ga can enhance their stability under operating reducing conditions, which would degrade and deactivate rapidly otherwise.[68] Based on that, metals with strong M–Cu bonding energies and high oxophilicity can be leveraged to develop stable alloyed CuSn-based electrocatalysts and hinder reconstruction over time. This strategy can ultimately protect the surface layer from Cu displacement due to ACN interaction and its stabilisation in the electrolyte solution due to triflate anions (see section. 3.2.4). A further mechanistic picture recently described the formation of $[CuCO]^+$ as the most favourable Cu-adsorbate complexes, regardless of the exposed copper surface, driving the dissolution.[69] The copper carbonyl is unstable and generally dissociates into Cu^+ and gaseous CO.[70].

Hence, a CuZn-based electrode[49] was investigated for the EC CO_2 conversion in [BMIM][TfO] in ACN solution as a counterproof. Although the CO to H_2 ratio was severely impacted, an interesting constant production of both products was reported at the current density of –20 mA cm^{-2}, with a final FE_{CO} higher than 10 % and a FE_{H2} of 50 % (**Fig. S11a** in SI). This finding indicates that, by catalyst reconstruction, zinc in the catalyst layer may help to stabilise Cu species against IL attack. Evidence of a possible Cu-Zn synergic effect in organic solutions may derive from the catalyst layer looking like the pristine electrode even after the test in **Fig. S11b** (SI). In this regard, some of us previously demonstrated that, in an aqueous electrolyte, the presence of ZnO in the Cu-based catalyst did not avoid the full catalyst reconstruction under CO_2 reduction conditions; flakes-like amorphous structures constituted by Zn containing metallic copper in bulk originated at –1.4 V vs. RHE.[49].

Whether the deactivation is linked to poisoning from IL-species adsorption on the Cu_2O/SnO_2 catalyst surface or to catalyst dissolution in the IL-based solutions (electrolyte colour change observed) is the question this work sought to answer. Consequently, the catalytic system was also investigated at the molecular level to gain more in-depth insights into the mechanisms based on the described findings. Moreover, to better elucidate the role of the carbon GDL degradation in the detected general instability, the electrochemical interfaces and the electrodes were characterised using spectroscopic and electron microscopy techniques (see section 3.2).

However, it is interesting to note that in all the discussed cases, the FE toward gaseous products did not exceed 60–65 % in the used aprotic media. This observation induces us to reflect on possible side products. For instance, oxalic acid can be originated via the dimerisation of two $CO_2^{\cdot-}$ radicals in non-aqueous electrolytes.[56] Furthermore, it is well known that even trace amounts of water can lead to forming formic acid in aprotic solvent due to the protonation of a $CO_2^{\cdot-}$ radical and the following electron transfer.[27,71] In the specific case of the present work, the proton source can be either the humid membrane or the H^+ ions coming from the water dissociation at the ions exchange layers' interface of the bipolar membrane. Control experiments in a nitrogen atmosphere were conducted to gain further insights into the phenomena occurring in our system (see Fig. S12). Specifically, chronopotentiometry measurements at −20 mA cm^{-2} were performed on the Cu_2O/SnO_2-GDE and on a Ti plate as a blank test. The different trends and FE_{H2} observed in the two cases led us to hypothesise that the missing current could also be directed toward the electrochemical hydrogenation of acetonitrile, as demonstrated in a previous work by Jiao and collaborators.[72] It is worth noting that this side reaction may represent a potential advantage of the process, providing an alternative pathway for acetonitrile valorisation. Indeed, the electrochemical reduction of ACN to ethylamine could offer a more environmentally sustainable route for converting this feedstock into value-added products. This is especially relevant in a context where excess acetonitrile is typically incinerated as fuel, contributing to significant NOx emissions, [73] and where selective ethylamine production has primarily been

achieved through expensive methods.[72].

Furthermore, to encourage future investigations which effectively meet sustainability goals and reduce reliance on precious metals, a control experiment with a bare Cu_2O/SnO_2 catalyst (i.e., without Ru and Re-based complexes) was conducted. It exhibited a sharper decay in performance over time compared to the system incorporating Ru and Re (see Fig. S13), suggesting a promoting/stabilizing effect of these complexes on the initial catalyst.

3.2. Understanding the origin of instabilities of Cu_2O/SnO_2–based GDEs in IL-ACN electrolyte

3.2.1. Pre- and post-mortem characterisation

The Cu_2O/SnO_2 electrodes were characterised as prepared and after the EC CO_2R in the binary ILs-organic solvent solution to analyse the structural evolution and the catalyst layer reconstruction. Fig. 6 shows the FESEM micrographs of the fresh and tested electrodes. It can be noted that the EC process induced particle restructuration and transformation into a more compact and continuous layer (see Fig. 6**b**). Moreover, the porous structure of the GDE seems to be covered with a dense and amorphous structure layer in contrast to the original fresh electrode, as shown in Fig. 6**a**. It could be attributed to the deposition of organic components deriving from the IL-ACN electrolyte solution. In this regard, Fig. 6**c** presents time-lapse images for the post-mortem GDE undergoing modification during the first 117 s of interaction between the electron beam and the sample, demonstrating the presence of an organic matrix. Indeed, the EDS analysis shows that the coating is a Cu-poor layer, made up mainly of C, F, O and S elements with O/S and F/O atomic ratios of 3.2 and 1.02, which reflect their ratios in the anion of [BMIM][TfO]. Although the elements mentioned above are also present in the Nafion ionomer of the catalytic ink, the EDS performed on the fresh electrode did not reveal the presence of sulphur. It might be a consequence of the low Nafion concentration in the catalyst layer, which is below the instrument's sensitivity.

XRD patterns of the electrodes before and after testing are compared to understand the evolution of the crystalline phases. As mentioned in section 2.2, it is worth noting that the ink deposition is conducted by placing the carbon paper on a heating plate. After deposition, it was kept on it for some minutes to guarantee complete solvent evaporation. Thus, it is hypothesised that the electrode's preparation influences the material's oxidation state. Additionally, factors such as redox reactions in the organic electrolyte and exposure to varying potentials during powder preparation could promote the formation of mixed copper species. Therefore, the crystalline phases of the fresh electrode were characterised to establish a baseline (Fig. 7**a**). The XRD pattern reveals distinct reflections corresponding to metallic Cu crystalline phase (JCPDS number: 01–004-0836), Cu_2O (JCPDS number: 01–077-0199), CuO (JCPDS number: 00–048-1548) and SnO_2 (JCPDS number: 01–077-0451) diffraction peaks, confirming the presence of mixed copper oxidation states in the catalyst layer. The XRD pattern of the spent electrode tested in the binary IL-ACN electrolyte indicates that the residual copper is present predominantly in the Cu_2O oxidation state form (see Fig. 7**c**). It suggests that during EC CO_2R in the presence of the [BMIM][TfO]-ACN electrolyte, the initial mix of oxidation states within the catalyst layer was partially reduced. However, metallic Cu was present in the fresh electrode, which is the most reduced form of this metal. Likely, metallic copper is less stable in the [BMIM][TfO]-ACN electrolyte and could dissolve in the solution, potentially explaining the colour change. Besides, XRD analysis on the backside of the GDE (Fig. 7**d**) and EDX measurements (see **Table S2** in SI) on the cross-section of the electrode confirmed the presence of Cu_2O element along the entire GDE thickness. SnO_2, another key electrode component, exhibited structural degradation during the EC CO_2R, likely through surface amorphisation or dissolution into the electrolyte. The destabilisation of SnO_2 appears to be facilitated by the extraction properties of the IL, emphasising the complex interactions between the electrode materials and the electrolyte. The XRD pattern of the spent Cu_2O/SnO_2-based electrode tested in potassium bicarbonate during 24 h (Fig. 7**b**) reveals distinct structural changes compared to those tested in the IL-ACN electrolyte. The analysis demonstrated that the crystalline phase

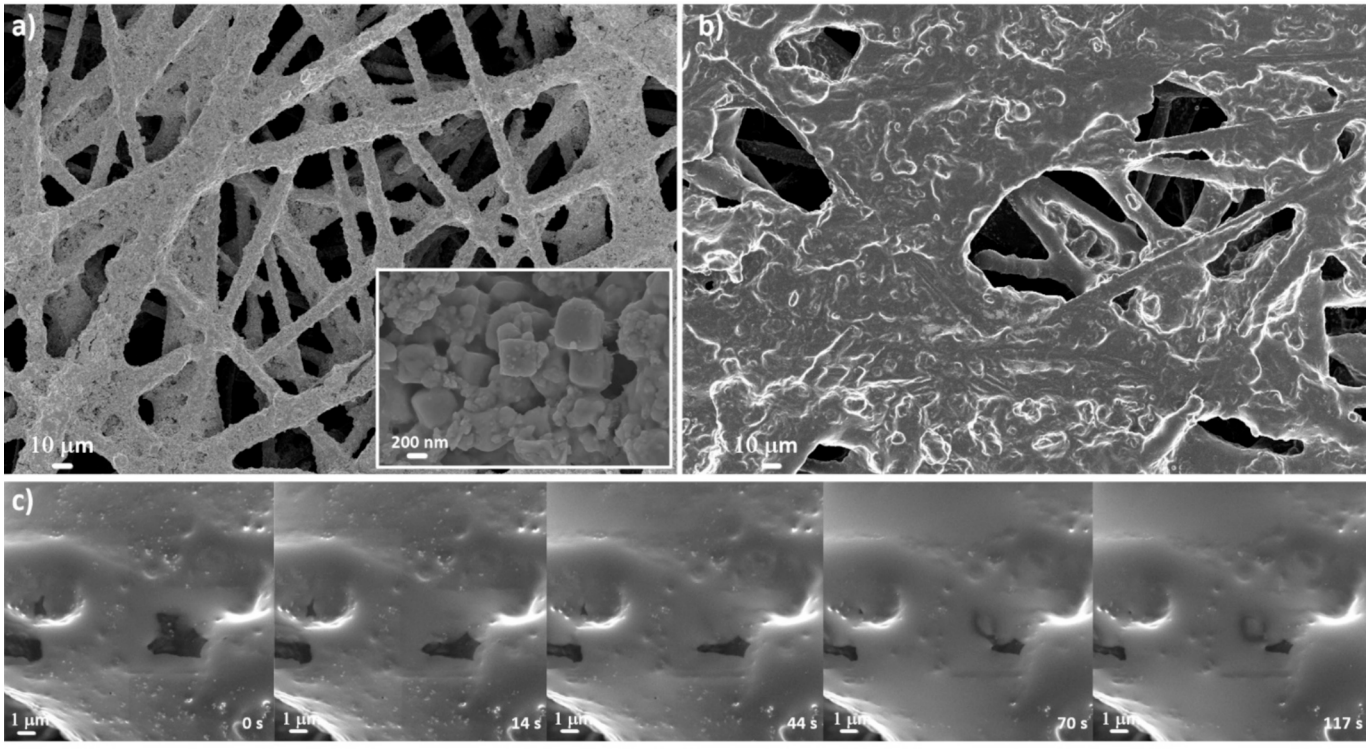

Fig. 6. FESEM images of (a) fresh and (b) tested Cu_2O/SnO_2-GDE in 0.3 M [BMIM][TfO] in acetonitrile solution. (c) Time-lapse FESEM images showing the surface modification after testing.

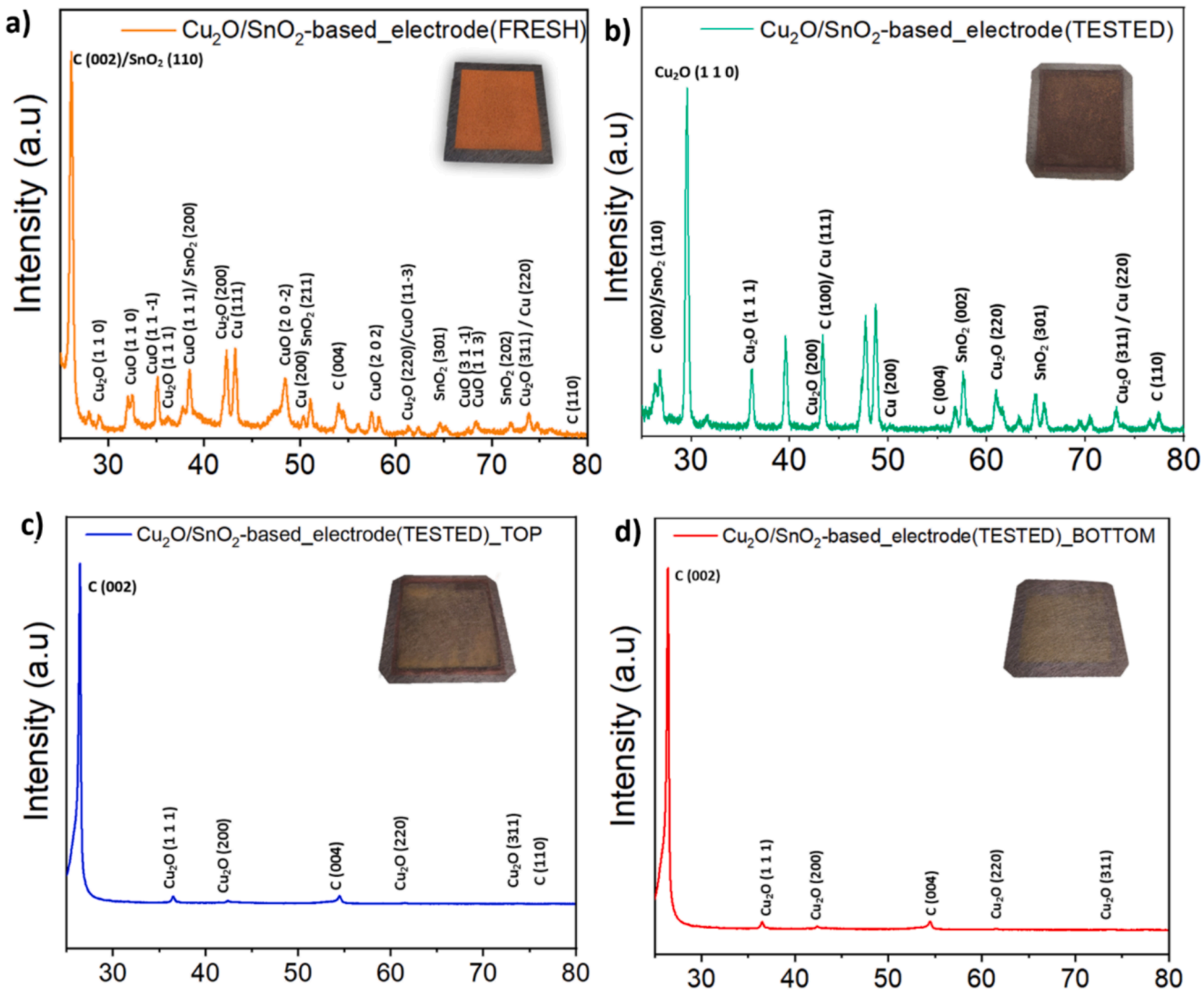

Fig. 7. XRD patterns of Cu_2O/SnO_2-GDE (a) fresh and (b) tested in $KHCO_3$ 0.1 M electrolyte; (c) (electrode top side) and (d) the carbon paper-side (electrode backside) of a Cu_2O/SnO_2-GDE after being tested in 0.3 M [BMIM][TfO] in acetonitrile solution.

composition changed during the electrochemical test, showing that CuO (Cu^{2+}) was entirely reduced. At the same time, the reflection peaks corresponding to SnO_2 were still present, suggesting its plausible role in stabilising the Cu_2O species and avoiding their complete reduction to metallic copper under CO_2 electroreduction conditions. In addition to the co-existence of metallic Cu and Cu_2O, other peaks were observed, which may be attributed to carbonate species, such as K_2CO_3, deposited on the catalyst surface after testing. This is consistent with previous reports, [74] suggesting that CuO can transform into copper hydroxy carbonates, such as malachite or azurite, during the electroreduction of CO_2 in water. The stabilisation of these species and the formation of Cu^+ (Cu_2O) likely contribute to the improved selectivity to CO by promoting favourable reaction pathways. These findings highlight the significant influence of electrolyte composition on catalyst surface transformation and performance during the reaction.

A control experiment using a CuO catalyst was conducted to better understand which oxidation state of copper promotes CO_2 reduction to CO in the presence of organic media. As hydrogen was the predominant gas-phase product (see Fig. S14), these results support the previously proposed hypothesis that Cu^+ species are essential for CO-selective behaviour, including in the [BMIM][TfO]/acetonitrile electrolyte. Furthermore, given that the dissolution of Cu is expected under these conditions – and its presence was not detected by post-test XRD analysis – we infer that metallic Cu does not play a significant role in CO production and that hydrogen and ethylamine[72] are likely the main products under these conditions.

3.2.2. *Electrochemical impedance spectroscopy analysis*

Electrochemical impedance spectroscopy is a powerful tool for studying the processes occurring at the electrode/electrolyte interfaces. It is widely used to study corrosion phenomena and the degradation of materials in harsh environments.[75–78] Therefore, after being operated under different reaction conditions, the EIS technique was adopted to deepen our understanding of the Cu_2O/SnO_2-GDE electrode behaviour over time.

In the aqueous electrolyte (Fig. 8**a-c**), comparing the EIS spectra after LSV, CP at –10 mA cm^{-2} and CP at –20 mA cm^{-2} revealed a stable behaviour over time. Indeed, the total impedance remained constant after each step, which agrees with the long-term stability of the GDE under these operative conditions. One process can be recognised at all the applied potentials by looking at the phase spectrum. As both the surface charge transfer and bulk charge transport are expected mechanisms, a possible explanation is that the two phenomena occur at the same time scale. A simple circuit was employed to fit the experimental data, constituted by the series resistance R_s (external electrical contacts, electrolyte and carbon paper) and by the parallel between the charge

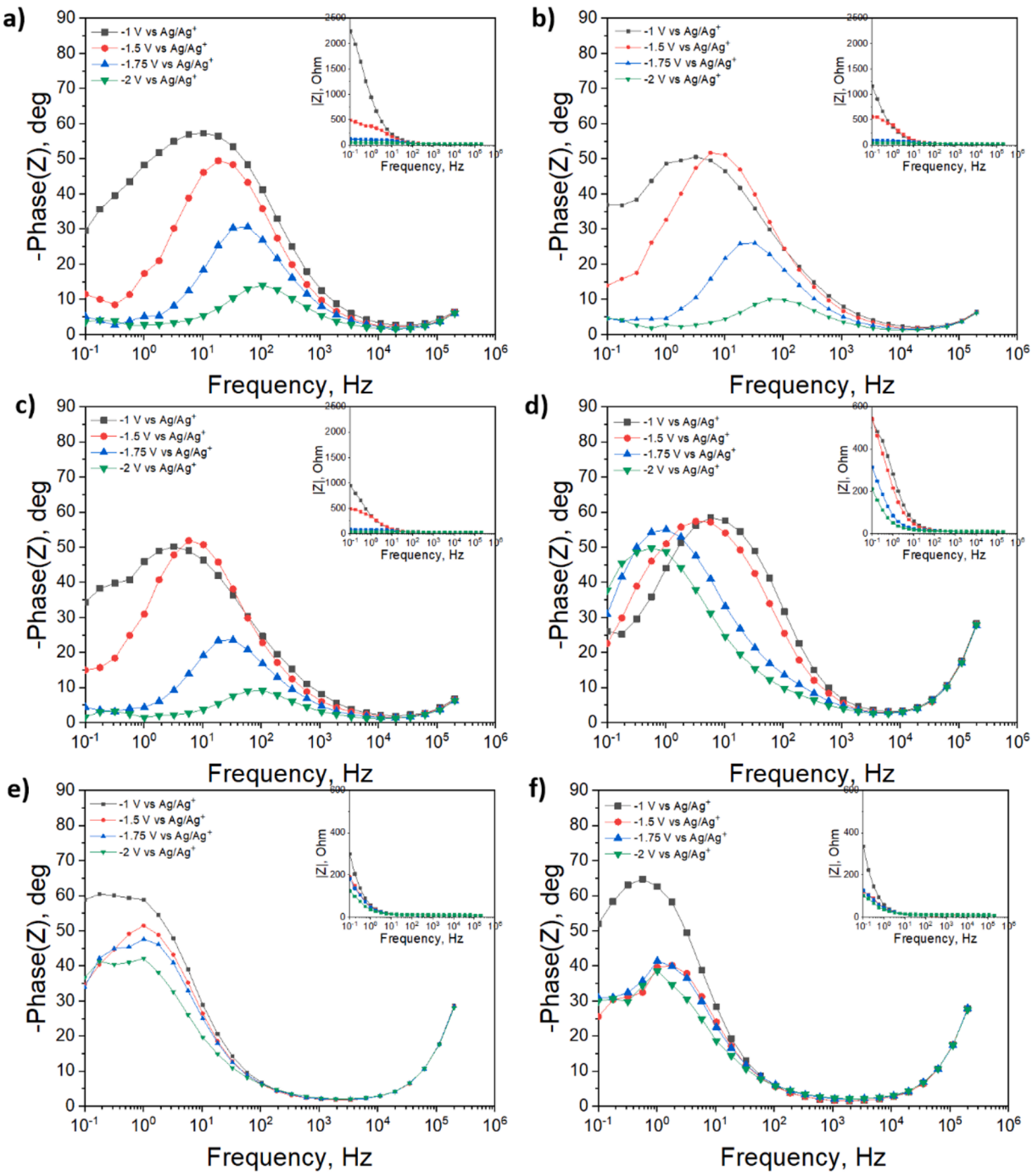

Fig. 8. EIS spectra performed on Cu_2O/SnO_2- GDEs in aqueous 0.1 M $KHCO_3$ (a, b, c) and in 0.3 M [BMIM][TfO] in ACN electrolytes (d, e, f) after LSV, CP at 10 mA cm^{-2} and CP at 20 mA cm^{-2}. The potential values are reported versus the $Ag/AgNO_3$ reference electrode.

transfer resistance R_{ct} and constant phase element Q_{ct} (R/CPE), used to describe the impedance at the catalyst/electrolyte interface. As can be seen from the superimposition of the EIS spectra collected after LSV in both solutions (Fig. S15 in SI), a good overlap between the fitting and experimental curves was obtained. The series resistance assumed values not dependent on the applied potentials were around 24Ω. Vice versa, the charge transfer resistance diminished upon increasing the applied potentials, reaching a minimum of 14Ω at –2V vs. $Ag/AgNO_3$ after CP at –20 mA cm^{-2}. The time constant of the charge transfer process was calculated through the following formula:

$$t_{ct} = (R_{ct}Q_{ct})^{1/n_{ct}} \quad (1)$$

where n_{ct} is the index of the constant phase element. In particular, the transfer of charges became faster at higher applied potentials, going from 35 to 1 ms (see Fig. S16 in SI).

Conversely, the EIS spectra related to the test in 0.3 M [BMIM][TfO] in ACN evidenced an unstable behaviour of the electrode throughout the electrochemical steps (Fig. 8**d-f**). The total impedance decreased over time at low overpotentials, which may be attributed to higher activity toward HER. On the contrary, what stands out immediately after watching the spectra after the CP measurements is that an additional process started occurring in the low-frequency region at higher overpotentials. A possible interpretation is that charge transfer and charge transport separate over time due to electrode degradation. Consistently

with this fact, another parallel R/CPE was used to interpret the new feature in the electrode's response. The interactions with the ILs-organic solvent solution led to a slowdown in the charge transfer process. That can be noticed by comparing the relative time constants from EIS measurements after the LSV and after CP at –20 mA cm^{-2} in **Fig. S16** (SI). For instance, at −2V vs. Ag/Ag^{+} the time constant changed from 400 ms to 1000 ms. It suggests that deactivation can be theorised during the electrochemical reaction with the Cu_2O/SnO_2-based catalyst in the presence of the [BMIM] [TfO] electrolyte, in agreement with the selectivity changes observed during the constant-current electrolysis experiments in section 3.1.

3.2.3. Morphology and surface characterisation

After the test in the IL-based electrolyte, either side of the electrodes darkened. Therefore, different spots of the tested GDE backside were examined at the field emission scanning electron microscope. The difference between an intact and a degraded area is striking. Fig. 9**a** shows how the PTFE coating of the fibres initially looked; Fig. 9**b** instead reveals the breakage of the PTFE treatment. It is evident that, during testing conditions, the PTFE coating is compromised by its interaction with the electrolyte solution. As further proof, EDS analysis detected fluorine in the different areas ranging from a mass percentage of about 48 % to less than 1 % (see **Table S3**). According to previous works, [79,80] the origin of the instabilities of carbon paper supports resides in the loss of the hydrophobic treatment, which directly exposes the unprotected fibres to the electrolyte solution and can provoke the mechanical/chemical degradation of the GDL. At higher overpotentials, the fibres exposed to the aggression of the organic-based electrolyte can be damaged and slow down the transport of electrons.

To further elucidate the causes of the GDL instability, Raman spectroscopy was used to characterise the carbon fibres before and after testing. Indeed, this spectroscopic technique finds extensive application in the analysis of carbon materials, providing valuable insights into defect density, disorder structures, and doping levels. Fig. 10 illustrates a comparison between the Raman spectra obtained from the ACN, [BMIM][TfO], and carbon fibres before and after testing at –20 mA cm^{-2} in the electrolyte solution of [BMIM][TfO] in ACN. The spectrum of the carbon fibres (collected in multiple points of the analysed surface) did not present any characteristic peak related to the ACN or the [BMIM][TfO] test solvent. The primary peaks observed at approximately 1315 cm^{-1}, 1585 cm^{-1}, and 2623 cm^{-1} correspond to the D band, G band, and 2D carbon peak, respectively. The D band represents disordered structures and defects in the graphitic material, while the G band is associated with ordered graphitic structure.[81] The ratio of the D band intensity to the G band intensity (I_D/I_G) can be considered as an indication of the level of disorder in a graphitic structure: a higher ratio suggests a highly disordered and defective crystal lattice, whereas a lower ratio implies a less defective and more ordered structure.[82] An analysis of the Raman spectra (Table 1) reveals that the carbon fibres exhibit an increased I_D/I_G ratio after testing, indicating higher lattice defects resulting from operating under electrochemical reduction conditions in the IL/organic electrolyte.[83] Moreover, the I_{2D}/I_G ratio was also evaluated. Indeed, in carbon materials, the 2D band is affected by electron–electron interactions and can be used to assess changes in charge carrier density.[84] Consequently, the ratio of the intensity of the 2D band to the G band (I_{2D}/I_G) might be associated with the carbon fibres' surface charge carrier density. After testing, the I_{2D}/I_G ratios collected in several points of the carbon fibres are higher than those obtained for the fresh carbon paper (Table 1). Thus, in addition to an increase in disorder indicated by the elevated I_D/I_G ratio, the interactions of the GDL with the ILs/organic electrolyte under electrochemical reduction conditions lead to a decrease in the charge carrier density. This finding proves an increased resistance to electron flow over time and as a consequence of the exposure of fibres to the organic environment, hence demonstrating the physical degradation of the GDL under reaction conditions suggested by the FESEM characterisation.

3.2.4. Theoretical investigation by ab initio molecular dynamics

It is generally accepted that adsorbed molecules on a catalytic surface can change surface structure and properties.[85–87] However, the mechanisms underlying these changes are unclear. Ab initio molecular dynamics is a powerful tool for understanding how a chemical system evolves at the molecular level and, in this context, investigating how and why adsorbed molecules can cause catalyst change and deactivation.

XRD analysis revealed the presence of metallic copper, Cu (111), and Cu_2O in the fresh electrode sample. Therefore, different systems were settled to investigate the interactions between the [BMIM][TfO] solution in ACN and the catalyst surface. First, it was studied how ACN, BMIM, and TfO molecules in different concentrations interact with a Cu (111) surface and then with a Cu_2O (100) surface.

The first observation from the simulations is the strong affinity between ACN molecules and copper (Fig. 11**a**). The stability of the copper FCC (111) surface is known to be very high.[88] It is experimentally observed that it does not undergo any restructuring at high temperatures, unlike the other stable Cu (100) facet, but passes directly from the solid to the liquid state once it has reached the melting point.[89,90] Surprisingly, the simulations demonstrate that ACN molecules could displace the Cu surface atoms from their equilibrium position in the (111) lattice. Fig. 11**b and c** report the population of copper atoms along the z-axis and the population of coordination numbers in the two top layers of the Cu surface. From these analyses, it is possible to observe how the presence of ACN in solution increases the population of Cu atoms with coordination numbers 6 and 11. This ability was also preserved in the presence of [BMIM][TfO]. In contrast, when the

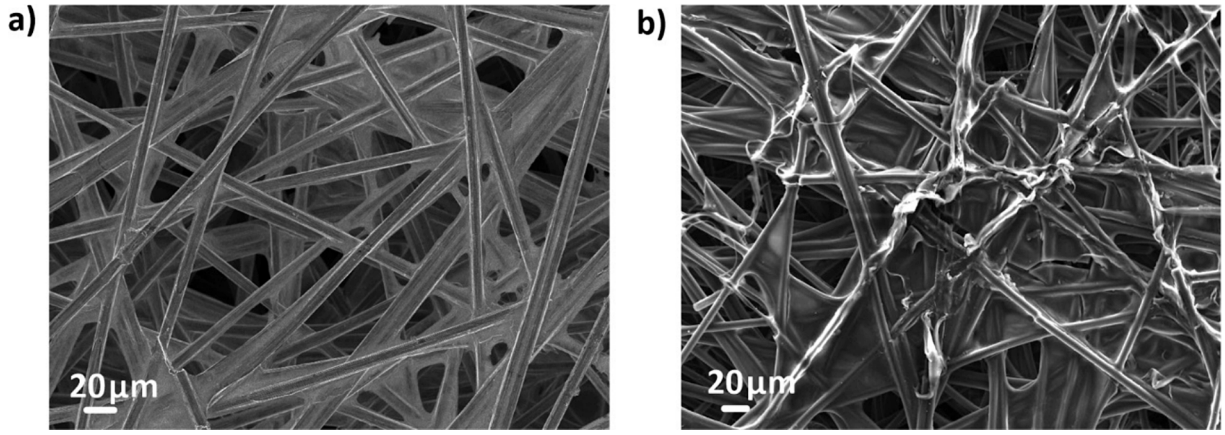

Fig. 9. FESEM micrographs of the backside of Cu_2O/SnO_2- GDE after test on intact (a) and degraded (b) areas.

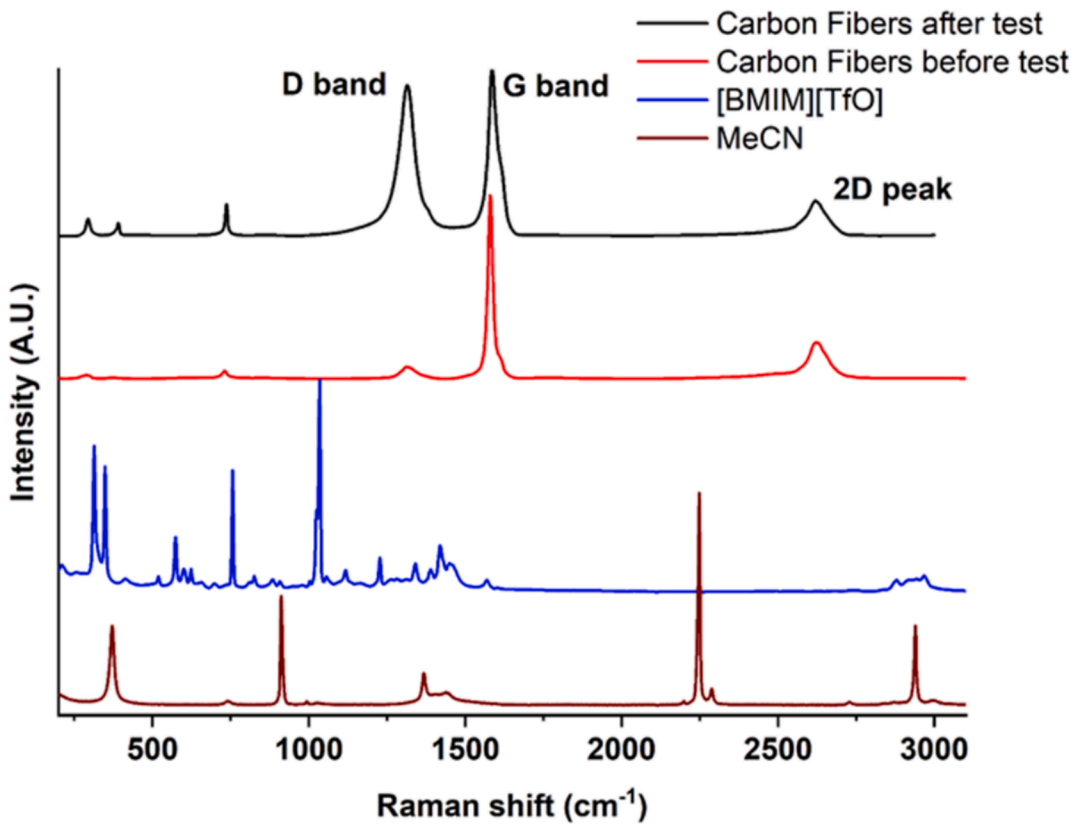

Fig. 10. Raman spectra of [BMIM][TfO], acetonitrile and carbon fibres before/after test.

Table 1
Parameters for Raman shifts of D, G, 2D and related intensities of the carbon fibres before and after the test.

	D Band shift (cm^{-1})	G Band shift (cm^{-1})	2D peak shift (cm^{-1})	I_D/I_G ratio	I_{2D}/I_G ratio
Carbon fibres before test	1318.8 ± 0.3	1580.0 ± 0.2	2626.0 ± 0.3	0.68 ± 0.04	0.73 ± 0.03
Carbon fibres after test	1312.9 ± 0.3	1589.2 ± 0.3	2621.0 ± 0.4	0.98 ± 0.05	0.82 ± 0.04

concentration of [BMIM][TfO] is higher than ACN (the Cu (111) + [BMIM][TfO] case in Fig. 11), any relevant displacement in the copper surface was observed, suggesting that IL molecules alone do not have the same ability of ACN to displace Cu atoms.

The same analyses were performed for the Cu_2O (100) surface (see **Fig. S17 in SI**). In this case, a displacement was not observed along the z-direction as strong as in the Cu (111) surface. However, a similar increment of low-coordinated Cu atoms on the surface was observed, with Cu-Cu coordination numbers passing from 8 to 6.

To further investigate the possibility of having dissolution of Cu atoms, a set of AIMD simulations of the Cu (111) and Cu_2O (100) surfaces were performed, with a vacancy and a Cu^+ ion in solution and with the same relative concentrations of ACN and [BMIM][TfO]. It is worth noting that this study was limited to analysing the relative stability of the two systems only in terms of potential energy difference to ascertain the thermodynamical feasibility of the process.

After reaching equilibrium, the average potential energy for the different systems was calculated, and the resulting values are reported in Table 2. From these calculations, it is noticed that only in the case of Cu (111) does the combined presence of ACN and [BMIM][TfO] molecules stabilise the Cu ion in the solution with respect to the pristine surface. The same does not occur for Cu_2O.

From these findings, it can be hypothesised that the combined presence of ACN and [BMIM][TfO] molecules destabilise the catalyst surface. It can be inferred that ACN is responsible for restructuring the surface and creating defects, while the presence of IL molecules (particularly [TfO]) stabilises the Cu ions in the solution. Moreover, under the EC CO_2R conditions, one can hypothesise that Cu_2O is reduced to metallic copper, which is more easily disordered and it subsequently dissolved in the solution.

3.2.5. *Remarks*

Our results demonstrate that the IL-ACN electrolyte system faces significant performance challenges. Notably, CO production rapidly declines, highlighting the system's current suboptimal performance compared to more established aqueous electrolytes. The observed decline can be attributed to the instability of the Cu-based GDE support in the aprotic environment and potential degradation mechanisms like Cu atom displacement, as confirmed by ex-situ characterisation and computational modelling. We recognise that these performance limitations could question the novelty and practicality of using IL-ACN electrolytes for continuous-flow CO_2 reduction systems. However, our study aims to comprehensively explore both the potential and limitations of IL-based electrolytes in continuous-flow CO_2 reduction systems to better inform future research and development. Despite these challenges, our investigation into IL-ACN electrolytes remains crucial. The rationale for continuing to investigate it lies in their unique properties, which could present advancement opportunities under optimised conditions. ILs have demonstrated the potential to modulate the local reaction environment, stabilise reactive intermediates, and provide wide electrochemical stability windows. These features may still be beneficial if catalyst stability and electrolyte composition challenges can be addressed. Furthermore, ILs offer a distinct advantage as dual-function materials that can capture and convert CO_2, which remains a compelling area of research despite current performance constraints. Our

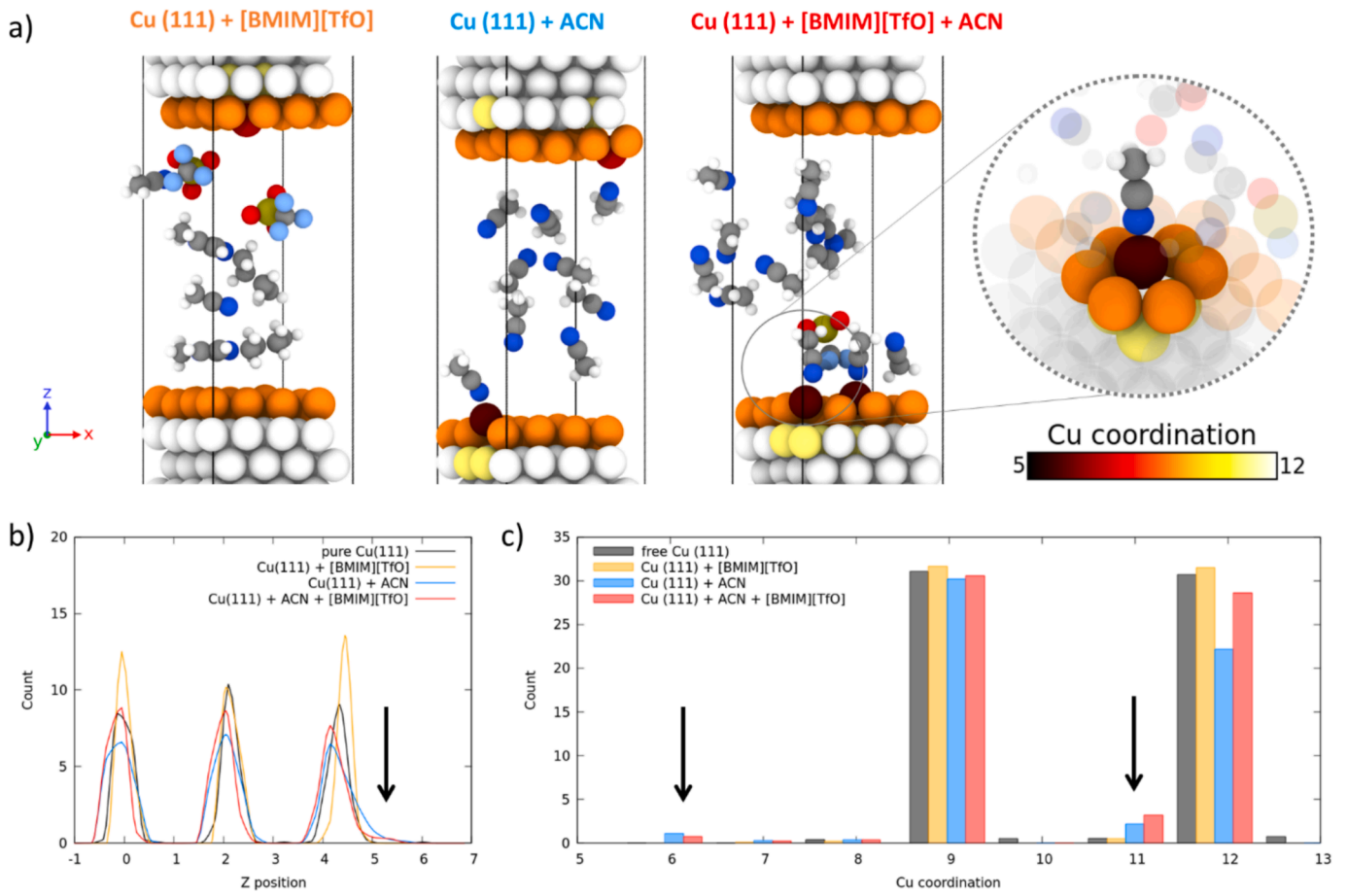

Fig. 11. (a) Snapshots of the three systems simulated for the Cu (111) surface. Atoms are coloured as follows: carbon in grey, hydrogen in white, nitrogen in blue, sulphur in yellow, oxygen in red, and fluorine in light blue. Copper atoms are coloured according to their coordination. (b) Copper population density function of the z direction. (c) coordination number population of the two top layers of the Cu surface.

Table 2
Averaged energy differences between the pristine systems and those with a copper atom removed from the surface and placed in the solution.

	Cu (111)		Cu_2O (100)	
	+ ACN	+ ACN + [BMIM][TfO]	+ ACN	+ ACN + [BMIM][TfO]
ΔE (kcal/mol)	6.9	0.1	34.3	26.5

findings also emphasise the critical issues that must be overcome to make IL-based electrolytes viable for industrial applications. By understanding degradation mechanisms, such as Cu atom displacement and electrode instability, this study can guide the research to tailor IL systems for better performance. For future optimisation, the ACN organic solvent can be replaced to prevent the displacement of Cu atoms to the catalyst surface, which is the first step for Cu dissolution in the aprotic electrolyte. Another helpful strategy could be the investigation of different IL anions that do not form complexes with Cu or Sn, thereby countering their stabilisation in the media. To achieve this, the recent work by Dattila *et al.*,[91] which outlines thermodynamic descriptors for screening different imidazolium-based ionic liquids and estimating their selectivity during the EC CO_2R reactions, can be implemented as a valuable tool for selecting the most appropriate IL for this purpose. Additionally, the application of ionomer or other metal oxide coatings that can strengthen and stabilise the oxidation phase of Cu on the GDE surface should be investigated for long-term operation with IL-based electrolytes. To further reduce reliance on precious metals and effectively address the sustainability aspect, future experiments should focus on engineering and stabilise the oxidation state of the Cu-based catalysts in order to achieve a stable and efficient match between the electrocatalyst and the organic electrolyte.

4. Conclusions

Ionic liquid's co-catalytic properties for CO_2 electroreduction have been exhibited in batch reactors. To our knowledge, only a few studies have tried to move towards continuous systems. Here, to increase the production rates and investigate the potential application of a low-cost electrode compared to the Ag- and Au-based state-of-the-art systems, the electrochemical conversion of CO_2 to syngas was performed on Cu_2O/SnO_2-based GDEs in a flow-continuous reactor. A promising selectivity of the Cu/Sn-based core–shell nanoparticles was revealed in an aqueous electrolyte ($KHCO_3$ 0.1 M), specifically achieving a CO to H_2 ratio of about 10. An outstanding FE_{CO} of 90 % was achieved, and its stability in a protic environment was demonstrated for 24 h at −20 mA cm^{-2}, while $FE_{CO} > 84$ % where obtained at higher relevant current densities of up to 100 mA cm^{-2}. The protic electrolyte was replaced by an organic (0.3 M [BMIM][TfO] in ACN) solution to boost the CO_2 conversion. The results revealed a CO-selective behaviour, which did not maintain a steady state. Indeed, H_2 became the major product over time, and a darkening of the GDE was observed. Accordingly, different

factors were examined experimentally to understand what underlies the unstable phenomena. Additionally, computational modelling at the molecular level sustains the hypothesis that the interactions with ACN molecules caused the decline in CO selectivity. The organic solvent promoted the destabilisation of Cu surface atoms and its consequent dissolution, favoured by the triflate anion of the IL. Experimentally, that was further confirmed by ex-situ XRD analysis. In turn, the described phenomenon caused the electrolyte colour change and exposed the carbon fibres to the aggression of the electrolyte, generating the support degradation. EIS, Raman and FESEM measurements corroborated the amorphisation and resistance increase of the carbon support. To the best of our knowledge, previous research on organic solvents has been focused on their use in batch reactors and with Cu foils as the cathodes. It showed CO as the main reaction product and the sensitivity of EC CO_2R in acetonitrile-based electrolytes to water. The work presented here aimed at initiating the scale-up of the CO_2R process in the presence of aprotic media in a flow system. Many degradation phenomena were reported, as well as efficiency loss over time. However, we wanted to investigate the origins of the instabilities to inform the research community and guide future work toward proper and crucial optimisation of the electrolyte solution. Understanding the mechanisms underlying instabilities is the first step to addressing the stability challenges. The results obtained in this study indicate that further efforts are needed to prepare the IL-based electrochemical systems for their scalability, while also promoting their use due to the potential impact of aprotic electrolytes on overall process performance. This ultimately paves the way for follow-up studies focussed on modifying electrolyte compositions, exploring protective coatings, or enhancing the robustness of catalysts to harness the potential benefits of IL-based systems fully. This study provides essential insights to determine whether IL-ACN electrolytes can be optimised for practical use and provide insights on alternative approaches that could be pursued.

CRediT authorship contribution statement

Federica Zammillo: Writing – original draft, Visualization, Methodology, Investigation, Data curation, Conceptualization. **Hilmar Guzmán:** Writing – original draft, Visualization, Validation, Methodology, Investigation, Conceptualization. **Daniela Polino:** Writing – original draft, Formal analysis. **Roger Miró:** Writing – original draft, Methodology, Investigation. **Alberto Lopera:** Writing – original draft, Methodology, Investigation. **Emmanuele Parisi:** Writing – original draft, Methodology, Investigation. **Alessia Fortunati:** Methodology, Investigation. **Maddalena Zoli:** Methodology, Investigation. **Elena Simone:** Supervision, Resources, Methodology. **Nunzio Russo:** Writing – review & editing, Supervision. **Mariajose López-Tendero:** Supervision, Resources, Methodology. **Miriam Díaz de los Bernardos:** Supervision, Resources, Methodology. **Giovanni M. Pavan:** Supervision, Resources, Methodology, Conceptualization. **Simelys Hernández:** Writing – review & editing, Validation, Supervision, Resources, Project administration, Methodology, Funding acquisition, Conceptualization.

Declaration of competing interest

The authors declare that they have no known competing financial interests or personal relationships that could have appeared to influence the work reported in this paper.

Acknowledgements

The research leading to these results has received funding from the European Union's Horizon 2020 Research and Innovation Action program under the SunCoChem project (Grant Agreement No 862192). GMP acknowledges the funding received by the European Research Council (ERC) under the European Union's Horizon 2020 research and innovation program (Grant Agreement No. 818776 - DYNAPOL). The authors also acknowledge the computational resources provided by the Swiss National Supercomputing Center (CSCS) under project s1226. ES acknowledges the funding received from the ERC under the European Union's Horizon 2020 research and innovation program (Grant Agreement No 949229 - CryForm). The authors want to thank IoLiTec GmbH for the supply of ionic liquids, Federico Dattila (https://orcid.org/0000-0001-8195-3951) and Eleonora Calì (https://orcid.org/0000-0001-8406-675X) for FESEM and EDX analysis, and Noemi Pirrone for the support in the analysis of XRD measurements. FZ thanks Fondazione CRT for the financial support.

Appendix A. Supplementary data

Supplementary data to this article can be found online at https://doi.org/10.1016/j.cej.2025.163265.

Data availability

All computational details on the simulations conducted in this work are provided in the Supplementary material. Complete details of all molecular models used for the simulations, of the simulation parameters (input files, etc.), and the analysis are available at: https://doi.org/10.5281/zenodo.15342815.

References

[1] IPCC, Climate Change 2014: Synthesis Report. Contribution of Working Groups I, II and III to the Fifth Assessment Report of the Intergovernmental Panel on Climate Change, Geneva, Switzerland, 2014.
[2] K. Malik, S. Singh, S. Basu, A. Verma, Electrochemical reduction of CO_2 for synthesis of green fuel, Wiley Interdiscip. Rev. Energy Environ. 6 (2017), https://doi.org/10.1002/wene.244.
[3] R.M. Cuéllar-Franca, A. Azapagic, Carbon capture, storage and utilisation technologies: A critical analysis and comparison of their life cycle environmental impacts, J. CO_2 Util. 9 (2015) 82–102, https://doi.org/10.1016/j.jcou.2014.12.001.
[4] N.S. Romero Cuellar, K. Wiesner-Fleischer, M. Fleischer, A. Rucki, O. Hinrichsen, Advantages of CO over CO_2 as reactant for electrochemical reduction to ethylene, ethanol and n-propanol on gas diffusion electrodes at high current densities, Electrochim. Acta 307 (2019) 164–175, https://doi.org/10.1016/j.electacta.2019.03.142.
[5] H. Guzmán, F. Zammillo, D. Roldán, C. Galletti, N. Russo, S. Hernández, Investigation of gas diffusion electrode systems for the electrochemical CO_2 conversion, Catalysts 11 (2021), https://doi.org/10.3390/catal11040482.
[6] S. Garg, M. Li, A.Z. Weber, L. Ge, L. Li, V. Rudolph, G. Wang, T.E. Rufford, Advances and challenges in electrochemical CO_2 reduction processes: An engineering and design perspective looking beyond new catalyst materials, J. Mater. Chem. A 8 (2020) 1511–1544, https://doi.org/10.1039/c9ta13298h.
[7] M. König, J. Vaes, E. Klemm, D. Pant, Solvents and Supporting Electrolytes in the Electrocatalytic Reduction of CO_2, Iscience 19 (2019) 135–160, https://doi.org/10.1016/j.isci.2019.07.014.
[8] S. Nitopi, E. Bertheussen, S.B. Scott, X. Liu, A.K. Engstfeld, S. Horch, B. Seger, I.E. L. Stephens, K. Chan, C. Hahn, J.K. Nørskov, T.F. Jaramillo, I. Chorkendorff, Progress and Perspectives of Electrochemical CO_2 Reduction on Copper in Aqueous Electrolyte, Chem. Rev. 119 (2019) 7610–7672, https://doi.org/10.1021/acs.chemrev.8b00705.
[9] P. Jeanty, C. Scherer, E. Magori, K. Wiesner-Fleischer, O. Hinrichsen, M. Fleischer, Upscaling and continuous operation of electrochemical CO_2 to CO conversion in aqueous solutions on silver gas diffusion electrodes, J. CO2 Util. 24 (2018) 454–462, https://doi.org/10.1016/j.jcou.2018.01.011.
[10] J. Albo, A. Irabien, Cu_2O-loaded gas diffusion electrodes for the continuous electrochemical reduction of CO_2 to methanol, J. Catal. 343 (2016) 232–239, https://doi.org/10.1016/j.jcat.2015.11.014.
[11] N. Gupta, M. Gattrell, B. MacDougall, Calculation for the cathode surface concentrations in the electrochemical reduction of CO_2 in $KHCO_3$ solutions, J. Appl. Electrochem. 36 (2006) 161–172, https://doi.org/10.1007/s10800-005-9058-y.
[12] J. Herranz, A. Pătru, E. Fabbri, T.J. Schmidt, Co-electrolysis of CO_2 and H_2O: From electrode reactions to cell-level development, Curr. Opin. Electrochem. 23 (2020) 89–95, https://doi.org/10.1016/j.coelec.2020.05.004.
[13] J.T. Song, H. Song, B. Kim, J. Oh, Towards higher rate electrochemical CO_2 conversion: From liquid-phase to gas-phase systems, Catalysts 9 (2019), https://doi.org/10.3390/catal9030224.
[14] T. Burdyny, W.A. Smith, CO_2 reduction on gas-diffusion electrodes and why catalytic performance must be assessed at commercially-relevant conditions, Energy Environ. Sci. 12 (2019) 1442–1453, https://doi.org/10.1039/c8ee03134g.

[15] M. Jouny, G.S. Hutchings, F. Jiao, Carbon monoxide electroreduction as an emerging platform for carbon utilization, Nat. Catal. 2 (2019) 1062–1070, https://doi.org/10.1038/s41929-019-0388-2.

[16] Y. Matsubara, Standard Electrode Potentials for the Reduction of CO_2 to CO in Acetonitrile-Water Mixtures Determined Using a Generalized Method for Proton-Coupled Electron-Transfer Reactions, ACS Energy Lett. 2 (2017) 1886–1891, https://doi.org/10.1021/acsenergylett.7b00548.

[17] X. Lu, D.Y.C. Leung, H. Wang, M.K.H. Leung, J. Xuan, Electrochemical Reduction of Carbon Dioxide to Formic Acid, ChemElectroChem 1 (2014) 836–849, https://doi.org/10.1002/celc.201300206.

[18] D. Faggion, W.D.G. Gonçalves, J. Dupont, CO_2 electroreduction in ionic liquids, Front. Chem. 7 (2019) 1–8, https://doi.org/10.3389/fchem.2019.00102.

[19] A. Hailu, S.K. Shaw, Efficient Electrocatalytic Reduction of Carbon Dioxide in 1-Ethyl-3-methylimidazolium Trifluoromethanesulfonate and Water Mixtures, Energy Fuel 32 (2018) 12695–12702, https://doi.org/10.1021/acs.energyfuels.8b02750.

[20] L. Fengyang, Ju; Jinjin, Zhang and Weiwei, Efficient Electrochemical Reduction of CO_2 to CO in Ionic Liquid / Propylene Carbonate Electrolyte on Ag Electrode, Catalysts 10 (2020) 1–14.

[21] B.A. Rosen, A. Salehi-Khojin, M.R. Thorson, W. Zhu, D.T. Whipple, P.J.A. Kenis, R. I. Masel, Ionic liquid-mediated selective conversion of CO_2 to CO at low overpotentials, Science (80-.). 334 (2011) 643–644. https://doi.org/10.1126/science.1209786.

[22] O. Yuksel Orhan, E. Alper, Kinetics of reaction between CO_2 and ionic liquid-carbon dioxide binding organic liquid hybrid systems: Analysis of gas-liquid absorption and stopped flow experiments, Chem. Eng. Sci. 170 (2017) 36–47, https://doi.org/10.1016/j.ces.2017.01.051.

[23] C. Ma, N. Wang, N. Ye, X. Ji, CO_2 capture using ionic liquid-based hybrid solvents from experiment to process evaluation, Appl. Energy 304 (2021) 117767, https://doi.org/10.1016/j.apenergy.2021.117767.

[24] B.A. Rosen, W. Zhu, G. Kaul, A. Salehi-Khojin, R.I. Masel, Water Enhancement of CO_2 Conversion on Silver in 1-Ethyl-3-Methylimidazolium Tetrafluoroborate, J. Electrochem. Soc. 160 (2013) H138–H141, https://doi.org/10.1149/2.004303jes.

[25] Y. Oh, X. Hu, Ionic liquids enhance the electrochemical CO_2 reduction catalyzed by MoO_2, Chem. Commun. 51 (2015) 13698–13701, https://doi.org/10.1039/c5cc05263g.

[26] A.V. Rudnev, K. Kiran, A. Cedeño López, A. Dutta, I. Gjuroski, J. Furrer, P. Broekmann, Enhanced electrocatalytic CO formation from CO_2 on nanostructured silver foam electrodes in ionic liquid/water mixtures, Electrochim. Acta 306 (2019) 245–253, https://doi.org/10.1016/j.electacta.2019.03.102.

[27] R. Miró, H. Guzmán, C. Godard, A. Gual, F. Zammillo, T.J.S. Schubert, B. Iliev, A. Chiodoni, S. Hernández, M.d., de los Bernardos, Solar-driven CO_2 reduction catalysed by hybrid supramolecular photocathodes and enhanced by ionic liquids, Catal. Sci. Technol. (2023) 1708–1717, https://doi.org/10.1039/d2cy01523d.

[28] R. Miró, E. Fernández-Llamazares, C. Godard, M. Díaz de los Bernardos, A. Gual,, Synergism between iron porphyrin and dicationic ionic liquids: tandem CO_2 electroreduction-carbonylation reactions, Chem. Commun. (2022), https://doi.org/10.1039/d2cc03641j.

[29] G. Iijima, T. Kitagawa, A. Katayama, T. Inomata, H. Yamaguchi, K. Suzuki, K. Hirata, Y. Hijikata, M. Ito, H. Masuda, CO_2 Reduction Promoted by Imidazole Supported on a Phosphonium-Type Ionic-Liquid-Modified Au Electrode at a Low Overpotential, ACS Catal. (2018), https://doi.org/10.1021/acscatal.7b03274.

[30] M. Zanatta, N.M. Simon, J. Dupont, The Nature of Carbon Dioxide in Bare Ionic Liquids, ChemSusChem (2020), https://doi.org/10.1002/cssc.202000574.

[31] Y. Hu, J. Feng, X. Zhang, H. Gao, S. Jin, L. Liu, W. Shen, Efficient Electrochemical Reduction of CO_2 to CO in Ionic Liquids, ChemistrySelect 6 (2021) 9873–9879, https://doi.org/10.1002/slct.202102825.

[32] V. Vedharathinam, Z. Qi, C. Horwood, B. Bourcier, M. Stadermann, J. Biener, M. Biener, Using a 3D Porous Flow-Through Electrode Geometry for High-Rate Electrochemical Reduction of CO_2 to CO in Ionic Liquid, ACS Catal. 9 (2019) 10605–10611, https://doi.org/10.1021/acscatal.9b03201.

[33] W. Lai, Y. Qiao, Y. Wang, H. Huang, Stability Issues in Electrochemical CO2 Reduction: Recent Advances in Fundamental Understanding and Design Strategies, Adv. Mater. (2023) 1–78, https://doi.org/10.1002/adma.202306288.

[34] T.N. Huan, P. Simon, G. Rousse, I. Génois, V. Artero, M. Fontecave, Porous dendritic copper: an electrocatalyst for highly selective CO_2 reduction to formate in water/ionic liquid electrolyte, Chem. Sci. (2016), https://doi.org/10.1039/c6sc03194c.

[35] R.L. Sacci, S. Velardo, L. Xiong, D.A. Lutterman, J. Rosenthal, Copper-tin alloys for the electrocatalytic reduction of CO_2 in an Imidazolium-Based Non-Aqueous Electrolyte in an imidazolium-based non-aqueous electrolyte, Energies (2019), https://doi.org/10.3390/en12163132.

[36] X. An, P. Wang, X. Ma, X. Du, X. Hao, Z. Yang, G. Guan, Application of ionic liquids in CO_2 capture and electrochemical reduction: A review, Carbon Resour. Convers. (2023), https://doi.org/10.1016/j.crcon.2023.02.003.

[37] Y. Sha, J. Zhang, X. Cheng, M. Xu, Z. Su, Y. Wang, J. Hu, B. Han, L. Zheng, Anchoring Ionic Liquid in Copper Electrocatalyst for Improving CO_2 Conversion to Ethylene, Angew. Chemie - Int. Ed. (2022), https://doi.org/10.1002/anie.202200039.

[38] H. Cai, H. Yang, J. Feng, K. Zhou, C. Liu, Q. Hu, C. He, Ionic Liquid-Induced Product Switching in CO_2 Electroreduction on Copper Reaction Interface, Adv. Funct. Mater. 2404102 (2024) 1–9, https://doi.org/10.1002/adfm.202404102.

[39] C. Deacon-Price, A.H.M. da Silva, C.S. Santana, M.T.M. Koper, A.C. Garcia, Solvent Effect on Electrochemical CO_2 Reduction Reaction on Nanostructured Copper Electrodes, J. Phys. Chem. C (2023), https://doi.org/10.1021/acs.jpcc.3c03257.

[40] M. König, J. Vaes, D. Pant, E. Klemm, Effect of Solvents on Aprotic CO2 Reduction: A Study on the Role of CO_2 Mass Transport in the Product Selectivity between Oxalate and Carbon Monoxide, J. Phys. Chem. C (2023), https://doi.org/10.1021/acs.jpcc.3c03992.

[41] M.T. Jensen, M.H. Rønne, A.K. Ravn, R.W. Juhl, D.U. Nielsen, X.M. Hu, S. U. Pedersen, K. Daasbjerg, T. Skrydstrup, Scalable carbon dioxide electroreduction coupled to carbonylation chemistry, Nat. Commun. (2017), https://doi.org/10.1038/s41467-017-00559-8.

[42] Photoelectrocatalytic device for SUN-driven CO2 conversion into green CHEMicals, EU Horizon 2020 project under grant agreement No. 862192, CORDIS - EU Res. Results (2020). https://doi.org/10.3030/862192.

[43] Y. Shi, C. Xia, Y. Huang, L. He, Electrochemical Approaches to Carbonylative Coupling Reactions, Chem. - an Asian J. (2021), https://doi.org/10.1002/asia.202100800.

[44] B. Kim, S. Ma, H.R. Molly Jhong, P.J.A. Kenis, Influence of dilute feed and pH on electrochemical reduction of CO_2 to CO on Ag in a continuous flow electrolyzer, Electrochim. Acta (2015), https://doi.org/10.1016/j.electacta.2015.03.064.

[45] S. Van Daele, L. Hintjens, S. Hoekx, B. Bohlen, S. Neukermans, N. Daems, J. Hereijgers, T. Breugelmans, How flue gas impurities affect the electrochemical reduction of CO_2 to CO and formate, Appl. Catal. B Environ. 341 (2024) 123345, https://doi.org/10.1016/j.apcatb.2023.123345.

[46] P.K. Sharma, S. Rasul, D. Li, E.H. Yu, Selective conversion of CO_2 to CO using earth abundant tin modified copper gas diffusion electrodes, Mater. Reports Energy (2023), https://doi.org/10.1016/j.matre.2023.100196.

[47] W. Ju, F. Jiang, H. Ma, Z. Pan, Y.B. Zhao, F. Pagani, D. Rentsch, J. Wang, C. Battaglia, Electrocatalytic Reduction of Gaseous CO_2 to CO on Sn/Cu-Nanofiber-Based Gas Diffusion Electrodes, Adv. Energy Mater. (2019), https://doi.org/10.1002/aenm.201901514.

[48] A. Fortunati, F. Risplendi, M. Re Fiorentin, G. Cicero, E. Parisi, M. Castellino, E. Simone, B. Iliev, T.J.S. Schubert, N. Russo, S. Hernández, Understanding the role of imidazolium-based ionic liquids in the electrochemical CO_2 reduction reaction, Commun. Chem. 6 (2023) 1–13, https://doi.org/10.1038/s42004-023-00875-9.

[49] H. Guzmán, F. Salomone, S. Bensaid, M. Castellino, N. Russo, S. Hernández, CO_2 Conversion to Alcohols over Cu/ZnO Catalysts: Prospective Synergies between Electrocatalytic and Thermocatalytic Routes, ACS Appl. Mater. Interfaces 14 (2022) 517–530, https://doi.org/10.1021/acsami.1c15871.

[50] T.D. Kühne, M. Iannuzzi, M. Del Ben, V.V. Rybkin, P. Seewald, F. Stein, T. Laino, R. Z. Khaliullin, O. Schütt, F. Schiffmann, D. Golze, J. Wilhelm, S. Chulkov, M. H. Bani-Hashemian, V. Weber, U. Borštnik, M. Taillefumier, A.S. Jakobovits, A. Lazzaro, H. Pabst, T. Müller, R. Schade, M. Guidon, S. Andermatt, N. Holmberg, G.K. Schenter, A. Hehn, A. Bussy, F. Belleflamme, G. Tabacchi, A. Glöß, M. Lass, I. Bethune, C.J. Mundy, C. Plessl, M. Watkins, J. VandeVondele, M. Krack, J. Hutter, CP2K: An electronic structure and molecular dynamics software package -Quickstep: Efficient and accurate electronic structure calculations, J. Chem. Phys. (2020), https://doi.org/10.1063/5.0007045.

[51] J.P. Perdew, K. Burke, M. Ernzerhof, Generalized gradient approximation made simple, PhysRevLett.7 (1996), https://doi.org/10.1103/PhysRevLett.77.3865.

[52] J. VandeVondele, J. Hutter, Gaussian basis sets for accurate calculations on molecular systems in gas and condensed phases, J. Chem. Phys. (2007), https://doi.org/10.1063/1.2770708.

[53] M. Krack, Pseudopotentials for H to Kr optimized for gradient-corrected exchange-correlation functionals, Theor. Chem. Acc. (2005), https://doi.org/10.1007/s00214-005-0655-y.

[54] S. Goedecker, M. Teter, Separable dual-space Gaussian pseudopotentials, Phys. Rev. B - Condens. Matter Mater. Phys. (1996), https://doi.org/10.1103/PhysRevB.54.1703.

[55] G. Bussi, D. Donadio, M. Parrinello, Canonical sampling through velocity rescaling, J. Chem. Phys. (2007), https://doi.org/10.1063/1.2408420.

[56] M. Moura de Salles Pupo, R. Kortlever, Electrolyte Effects on the Electrochemical Reduction of CO_2, ChemPhysChem 20 (2019) 2926–2935, https://doi.org/10.1002/cphc.201900680.

[57] M.A. Blommaert, S. Subramanian, K. Yang, W.A. Smith, D.A. Vermaas, High Indirect Energy Consumption in AEM-Based CO_2 Electrolyzers Demonstrates the Potential of Bipolar Membranes, ACS Appl. Mater. Interfaces 14 (2022) 557–563, https://doi.org/10.1021/acsami.1c16513.

[58] N.T. Nesbitt, T. Burdyny, H. Simonson, D. Salvatore, D. Bohra, R. Kas, W.A. Smith, Liquid-Solid Boundaries Dominate Activity of CO_2 Reduction on Gas-Diffusion Electrodes, ACS Catal. 10 (2020) 14093–14106, https://doi.org/10.1021/acscatal.0c03319.

[59] M.C. Figueiredo, I. Ledezma-Yanez, M.T.M. Koper, In Situ Spectroscopic Study of CO_2 Electroreduction at Copper Electrodes in Acetonitrile, ACS Catal. 6 (2016) 2382–2392, https://doi.org/10.1021/acscatal.5b02543.

[60] B. De Mot, J. Hereijgers, M. Duarte, T. Breugelmans, Influence of flow and pressure distribution inside a gas diffusion electrode on the performance of a flow-by CO_2 electrolyzer, Chem. Eng. J. (2019), https://doi.org/10.1016/j.cej.2019.122224.

[61] U.O. Nwabara, M.P. De Heer, E.R. Cofell, S. Verma, E. Negro, P.J.A. Kenis, Towards accelerated durability testing protocols for CO_2 electrolysis, J. Mater. Chem. A (2020), https://doi.org/10.1039/d0ta08695a.

[62] S. Verma, U.O. Nwabara, P.J.A. Kenis, Carbon-Based Electrodes and Catalysts for the Electroreduction of Carbon Dioxide (CO_2) to Value-Added Chemicals, In (2019), https://doi.org/10.1007/978-3-319-92917-0_10.

[63] P. Wilde, P.B. O'Mara, J.R.C. Junqueira, T. Tarnev, T.M. Benedetti, C. Andronescu, Y.T. Chen, R.D. Tilley, W. Schuhmann, J.J. Gooding, Is Cu instability during the CO_2 reduction reaction governed by the applied potential or the local CO concentration? Chem. Sci. 12 (2021) 4028–4033, https://doi.org/10.1039/d0sc05990k.

[64] C.H.C. Janssen, A. Sánchez, G.J. Witkamp, M.N. Kobrak, A novel mechanism for the extraction of metals from water to ionic liquids, ChemPhysChem (2013), https://doi.org/10.1002/cphc.201300686.
[65] N. Papaiconomou, J.M. Lee, J. Salminen, M. Von Stosch, J.M. Prausnitz, Selective extraction of copper, mercury, silver, and palladium ions from water using hydrophobic ionic liquids, Ind. Eng. Chem. Res. (2008), https://doi.org/10.1021/ie0706562.
[66] W. Drisdell, S.H. Lee, D. Lee, D. Larson, H. Li, J. Chen, S. Blair, A. Gallo, H. Zheng, C. Tassone, T. Jaramillo, Structural Transformation and Degradation of Cu Nanocatalysts during Electrochemical CO2 Reduction Reaction, Preprint (2023) 1–21. https://doi.org/10.21203/rs.3.rs-3204416/v1.
[67] C. Kim, J.C. Bui, X. Luo, J.K. Cooper, A. Kusoglu, A.Z. Weber, A.T. Bell, Tailored catalyst microenvironments for CO_2 electroreduction to multicarbon products on copper using bilayer ionomer coatings, Nat. Energy (2021), https://doi.org/10.1038/s41560-021-00920-8.
[68] V. Okatenko, A. Loiudice, M.A. Newton, D.C. Stoian, A. Blokhina, A.N. Chen, K. Rossi, R. Buonsanti, Alloying as a Strategy to Boost the Stability of Copper Nanocatalysts during the Electrochemical CO_2 Reduction Reaction, J. Am. Chem. Soc. (2023), https://doi.org/10.1021/jacs.2c13437.
[69] J. Vavra, G.P.L. Ramona, F. Dattila, A. Kormányos, T. Priamushk, P. Albertini, A. Loiudice, S. Cherevko, N. Lopéz, R. Buonsanti, Cu+ transient species mediate the reconstruction of copper electrocatalysts for CO2 reduction, Preprint (2022). https://doi.org/10.26434/chemrxiv-2022-3cr9k.
[70] M. Pasquali, C. Floriani, A. Gaetani-Manfredotti, Carbon Monoxide Absorption by Copper(I) Halides in Organic Solvents: Isolation and Structure of μ-Halogeno-dicopper(I) Carbonyl Complexes, Inorg. Chem. (1981), https://doi.org/10.1021/ic50224a046.
[71] C. Amatore, J.M. Savéant, Mechanism and Kinetic Characteristics of the Electrochemical Reduction of Carbon Dioxide in Media of Low Proton Availability, J. Am. Chem. Soc. 103 (1981) 5021–5023, https://doi.org/10.1021/ja00407a008.
[72] R. Xia, D. Tian, S. Kattel, B. Hasa, H. Shin, X. Ma, J.G. Chen, F. Jiao, Electrochemical reduction of acetonitrile to ethylamine, Nat. Commun. (2021), https://doi.org/10.1038/s41467-021-22291-0.
[73] P. Roose, K. Eller, E. Henkes, R. Rossbacher, H. Höke, Amines, Aliphatic in Ullmann's Encyclopedia of Industrial, Chemistry (2015).
[74] J. Albo, D. Vallejo, G. Beobide, O. Castillo, P. Castaño, A. Irabien, Copper-Based Metal–Organic Porous Materials for CO_2 Electrocatalytic Reduction to Alcohols, ChemSusChem (2017), https://doi.org/10.1002/cssc.201600693.
[75] S. Hernández, G. Gerardi, K. Bejtka, A. Fina, N. Russo, Evaluation of the charge transfer kinetics of spin-coated BiVO4 thin films for sun-driven water photoelectrolysis, Appl. Catal. B Environ. 190 (2016) 66–74, https://doi.org/10.1016/j.apcatb.2016.02.059.
[76] S. Hernández, S.M. Thalluri, A. Sacco, S. Bensaid, G. Saracco, N. Russo, Photo-catalytic activity of $BiVO_4$ thin-film electrodes for solar-driven water splitting, Appl. Catal. A Gen. 504 (2015) 266–271, https://doi.org/10.1016/j.apcata.2015.01.019.
[77] S. Hernández, G. Saracco, A.L. Alexe-Ionescu, G. Barbero, Electric investigation of a photo-electrochemical water splitting device based on a proton exchange membrane within drilled FTO-covered quartz electrodes: Under dark and light conditions, Electrochim. Acta 144 (2014) 352–360, https://doi.org/10.1016/j.electacta.2014.08.057.
[78] A. Sanginario, S. Hernández, Diagnostics of electrocatalytic systems by electrochemical impedance spectroscopy, Curr. Opin. Green Sustain. Chem. (2023), https://doi.org/10.1016/j.cogsc.2022.100727.
[79] K. Yang, R. Kas, W.A. Smith, T. Burdyny, Role of the Carbon-Based Gas Diffusion Layer on Flooding in a Gas Diffusion Electrode Cell for Electrochemical CO_2 Reduction, ACS Energy Lett. 6 (2021) 33–40, https://doi.org/10.1021/acsenergylett.0c02184.
[80] J. Park, H. Oh, T. Ha, Y. Il Lee, K. Min, A review of the gas diffusion layer in proton exchange membrane fuel cells, Durability and Degradation, Appl. Energy 155 (2015) 866–880, https://doi.org/10.1016/j.apenergy.2015.06.068.
[81] M.A. Pimenta, G. Dresselhaus, M.S. Dresselhaus, L.G. Cançado, A. Jorio, R. Saito, Studying disorder in graphite-based systems by Raman spectroscopy, Phys. Chem. Chem. Phys. 9 (2007) 1276–1291, https://doi.org/10.1039/b613962k.
[82] T. Maneerung, J. Liew, Y. Dai, S. Kawi, C. Chong, C.H. Wang, Activated carbon derived from carbon residue from biomass gasification and its application for dye adsorption: Kinetics, isotherms and thermodynamic studies, Bioresour. Technol. 200 (2016) 350–359, https://doi.org/10.1016/j.biortech.2015.10.047.
[83] A.K. Singh, M. Pahlevaninezhad, N. Yasri, E.P.L. Roberts, Degradation of Carbon Electrodes in the All-Vanadium Redox Flow Battery, ChemSusChem 14 (2021) 2100–2111, https://doi.org/10.1002/cssc.202100082.
[84] A. Das, S. Pisana, B. Chakraborty, S. Piscanec, S.K. Saha, U.V. Waghmare, K. S. Novoselov, H.R. Krishnamurthy, A.K. Geim, A.C. Ferrari, A.K. Sood, Monitoring dopants by Raman scattering in an electrochemically top-gated graphene transistor, Nat. Nanotechnol. 3 (2008) 210–215, https://doi.org/10.1038/nnano.2008.67.
[85] P. Grosse, D. Gao, F. Scholten, I. Sinev, H. Mistry, B. Roldan Cuenya, Dynamic Changes in the Structure, Chemical State and Catalytic Selectivity of Cu Nanocubes during CO_2 Electroreduction, Size and Support Effects, Angew. Chemie - Int. Ed. (2018), https://doi.org/10.1002/anie.201802083.
[86] P. Grosse, A. Yoon, C. Rettenmaier, A. Herzog, S.W. Chee, B. Roldan Cuenya, Dynamic transformation of cubic copper catalysts during CO_2 electroreduction and its impact on catalytic selectivity, Nat. Commun. (2021), https://doi.org/10.1038/s41467-021-26743-5.
[87] D. Gao, I. Sinev, F. Scholten, R.M. Arán-Ais, N.J. Divins, K. Kvashnina, J. Timoshenko, B. Roldan Cuenya, Selective CO_2 Electroreduction to Ethylene and Multicarbon Alcohols via Electrolyte-Driven Nanostructuring, Angew. Chemie - Int. Ed. (2019), https://doi.org/10.1002/anie.201910155.
[88] M. Cioni, D. Polino, D. Rapetti, L. Pesce, M. Delle Piane, G.M. Pavan, Innate Dynamics and Identity Crisis of a Metal Surface Unveiled by Machine Learning of Atomic Environments, J. Chem. Phys. (2023), https://doi.org/10.1063/5.0139010.
[89] A.N. Al-Rawi, A. Kara, T.S. Rahman, Comparative study of anharmonicity: Ni(111), Cu(111), and Ag(111), Phys. Rev. B - Condens. Matter Mater, Phys, 2002.
[90] K. Chae, H. Lu, T. Gustafsson, Medium-energy ion-scattering study of the temperature dependence of the structure of Cu(111), Phys. Rev. B - Condens. Matter Mater. Phys. (1996), https://doi.org/10.1103/PhysRevB.54.14082.
[91] F. Dattila, A. Fortunati, F. Zammillo, H. Guzmán, N. Núria López, S. Hernández, Descriptors for Electrochemical CO_2 Reduction in Imidazolium-Based Electrolytes, ACS Catal. (2024), https://doi.org/10.1021/acscatal.4c05012.